Lithos 340–341 (2019) 20–33

Contents lists available at ScienceDirect

Lithos

journal homepage: www.elsevier.com/locate/lithos

Insights on the origin of the Graciosa A-type granites and syenites (Southern Brazil) from zircon U-Pb geochronology, chemistry, and Hf and O isotope compositions

Frederico Castro Jobim Vilalva [a,*], Antonio Simonetti [b], Silvio Roberto Farias Vlach [c]

[a] Departamento de Geologia, Centro de Ciências Exatas e da Terra, Universidade Federal do Rio Grande do Norte, Natal, RN 59078-970, Brazil
[b] Department of Civil and Environmental Engineering and Earth Sciences, University of Notre Dame, Notre Dame, IN 46556, USA
[c] Departamento de Mineralogia e Geotectônica, Instituto de Geociências, Universidade de São Paulo, São Paulo, SP 05508-080, Brazil

ARTICLE INFO

Article history:
Received 25 March 2019
Accepted 3 May 2019
Available online 07 May 2019

Keywords:
Zircon
Trace element composition
U-Pb dating
Hf and O isotope geochemistry
A-type magmatism
Graciosa Province

ABSTRACT

The Neoproterozoic, post-collisional, Graciosa Province (southern Brazil) comprises several A-type intrusions and related volcanics of alkaline and subalkaline (or aluminous) petrographic associations. U-Pb age determinations, trace element, and Hf and O isotopic compositions were obtained for zircons from six distinct A-type granitic and syenitic plutons from both alkaline and subalkaline associations from the province. Geochronological results indicate that their emplacement, petrogenetic evolution and crystallization spanned over a ~9 million years interval, with peak magmatism at ~580 Ma. Plutons were emplaced in a post-collisional extensional regime related to the geodynamic evolution of the south-southeastern part of the Gondwana supercontinent. Hf isotopic compositions are highly variable, with εHf(t) values between +1.4 to −31, whereas $\delta^{18}O$ signatures are mainly between +4.7 and +6.0‰. These features, along with trace element signatures, especially for Hf, U, Nb, and rare-earth elements, suggest that generation of the Graciosa rocks occurred via partial melting of a lithospheric mantle previously metasomatized by slab-derived fluids, followed by variable degrees of crustal contamination at depth.

1. Introduction

According to Liégeois (1998), post-collisional geodynamic settings may include many geological events within a continuous or episodic extensional regime, where various types of magmatism can occur. A-type magmatism, in addition to being typical of anorogenic environments, has been consistently associated with extensional post-collisional settings (Bonin, 2007). Furthermore, the diversity of granitic rocks grouped under the A-type label, including peralkaline, metaluminous and even peraluminous varieties, renders it difficult to establish a common geological model for their generation. Unique crustal or mantle sources (or a mixture of both) have been invoked, but it seems most likely that a variety of source rocks and processes are involved in their generation (Bonin, 2007; Eby, 1992; Frost and Frost, 2011).

The abundance of A-type intrusive bodies within the Graciosa Province, southern Brazil (Gualda and Vlach, 2007a) provides an ideal setting to investigate the petrogenesis, evolution, composition and geotectonic significance of A-type granites. The Graciosa Province formed in an extensional, post-collisional regime that followed the amalgamation of Gondwana at the waning stages of the Brasiliano/Pan-African Orogeny in the Ediacaran Period. The province has been the focus of petrographic, mineralogical, chemical, isotopic, and geochronological studies over the last few decades that yielded a significant amount of data (e.g. Basei et al., 2009; Gualda and Vlach, 2007b; Vilalva and Vlach, 2014; Vlach et al., 2011; Vlach and Gualda, 2007). Nevertheless, the time span of the magmatism, the main petrological processes and differentiation mechanisms, as well as the tectonics involved are still matter of debate.

This study presents a combined investigation involving in-situ LA-ICP-MS U-Pb dating, trace element, and Hf and O isotopic compositions of zircon from six selected A-type granitic and syenitic plutons. Our results offer new insights into the timing of emplacement/crystallization, petrogenesis and evolution of the magmas, and the relationship with the geodynamic settings during the latter stages of the Brasiliano/Pan-African Orogeny in southern Brazil.

2. Geological background

The Graciosa Province consists of several post-collisional A-type granitic and syenitic plutons showing roughly circular to irregular outlines, as well as associated basic, intermediate and acid volcanics, gabbros, K-rich diorites and monzodiorites, as well as hybrid rocks. The plutons intruded at shallow crustal levels the Archean rocks of the Luis Alves Microplate, and Paleo- to Neoproterozoic rocks of the Curitiba

* Corresponding author.
E-mail addresses: frederico@geologia.ufrn.br (F.C.J. Vilalva), simonetti.3@nd.edu (A. Simonetti), srfvlach@usp.br (S.R.F. Vlach).

Microplate and Paranaguá Terrain (Fig. 1; Basei et al., 2009; Gualda and Vlach, 2007a; Passarelli et al., 2018; Siga Jr et al., 1993).

The Graciosa A-type granites and syenites are grouped into two distinct primary petrographic associations (Gualda and Vlach, 2007b). The *alkaline association* is composed of metaluminous alkali feldspar syenites to peralkaline hypersolvus granites formed under relatively reducing conditions, close to the fayalite-quartz-magnetite (FQM) buffer. In contrast, the *aluminous* (or *subalkaline* as used herein) *association* comprises metaluminous to moderately peraluminous subsolvus syeno- and monzogranites formed under more oxidizing conditions (Gualda and Vlach, 2007a; Vlach and Gualda, 2007). Rapakivi textures are occasionally noted. The main geochemical characteristics of the Graciosa Province are presented in Gualda and Vlach (2007a, 2007b), Kaul and Cordani (2000), Vlach and Gualda (2007), Vilalva and Vlach (2014), and references therein. In general, they all show affinities with the A2 subtype of Eby (1992) (Fig. 2a).

3. Samples

Nine samples were selected for this study, which represent granite and syenite varieties from both alkaline and subalkaline associations. Samples of the alkaline association are from the Papanduva (within the Morro Redondo Complex) and Corupá plutons, and Mandira Massif. Samples of the subalkaline association are from the Quiriri (within the Morro Redondo Complex) and Desemborque (within the Guaraú Massif) plutons, and Alto Turvo Massif (Fig. 1).

3.1. Alkaline association

Samples from the Papanduva Pluton (MR-39) and Mandira Massif (MAN-13A) are massive, holo- to leucocratic (color index: M' < 5) light-gray colored, fine- to medium-grained, hypersolvus alkali feldspar granites. Mafic minerals are arfvedsonite and riebeckite; aegirine occurs only in the Papanduva Pluton. Accessory minerals include astrophyllite, zircon and chevkinite, as well as a variety of rare HFSE-rich phases, mainly in the Papanduva Pluton, such as aenigmatite, britholite-(Ce), nacareniobsite-(Ce) and narsarsukite (Vilalva and Vlach, 2014). These are ferroan, peralkaline granites, with Fe* number [$FeO^T/(FeO^T + MgO)$, oxide wt%; Frost et al., 2001] = 0.97; A/CNK [molar $Al_2O_3/(CaO + Na_2O + K_2O)$] = 0.94; and A/NK [molar $Al_2O_3/(Na_2O + K_2O)$] = 0.96.

Samples CO-38, CO-32C and CO-32D, from the Corupá Pluton, represent different varieties of massive, medium- to coarse-grained, hypersolvus alkali feldspar syenites (Fig. 1). Sample CO-38 is an oversaturated (SiO_2 = 66.3 wt%), pink-colored, quartz alkali feldspar syenite with hedenbergite to aegirine-augite, and calcic to sodic-calcic

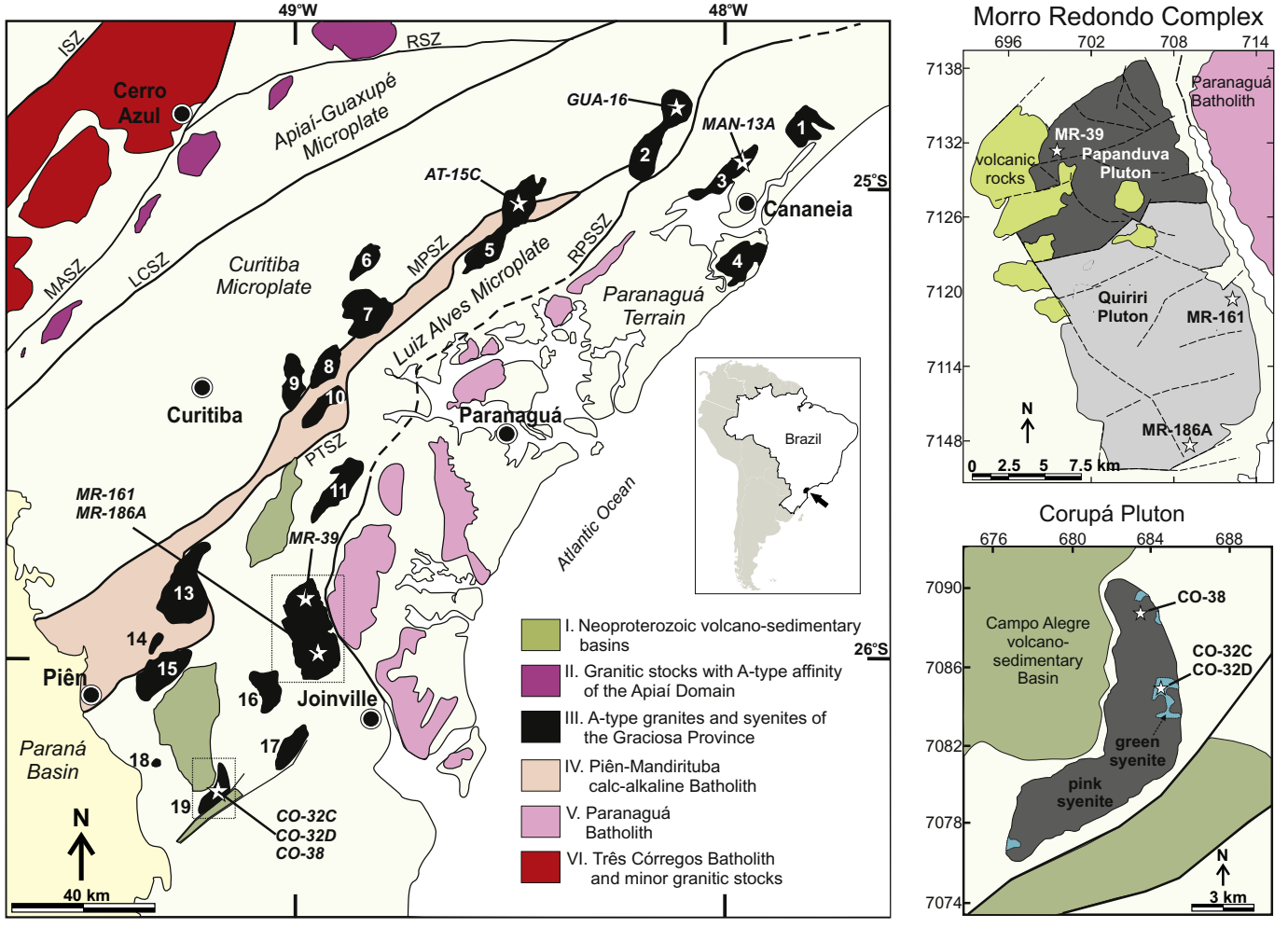

Fig. 1. Geological sketch of Southern Brazil, between the states of São Paulo (to the north) and Santa Catarina (to the south), showing the distribution of the plutons that form the Ediacaran A-type Graciosa Province, and the location of the studied samples (white stars). A-type granites and syenites of the Graciosa Province are: (1) Serra do Paratiú/Cordeiro; (2) Guaraú Massif (Desemborque Pluton); (3) Mandira; (4) Ilha do Cardoso; (5) Alto Turvo; (6) Capivari; (7) Órgãos; (8) Farinha Seca; (9) Anhangava; (10) Marumbi; (11) Serra da Igreja; (12) Morro Redondo Complex (Papanduva and Quiriri Plutons); (13) Palermo; (14) Agudos do Sul; (15) Rio Negro; (16) Dona Francisca; (17) Piraí; (18) Serra Alta; (19) Corupá. Simplified geological maps for the Morro Redondo Complex (Papanduva and Quiriri plutons) and Corupá Pluton, where more than one sample was analyzed, are also shown. Shear Zones (SZ): Itapirapuã (ISZ); Morro Agudo (MASZ); Ribeira (RPZ); Lancinha-Cubatão (LCSZ); Mandirituba-Piraquara (MPSZ); Piên-Tijucas (PTSZ); Rio Palmital-Serrinha (RPSSZ).

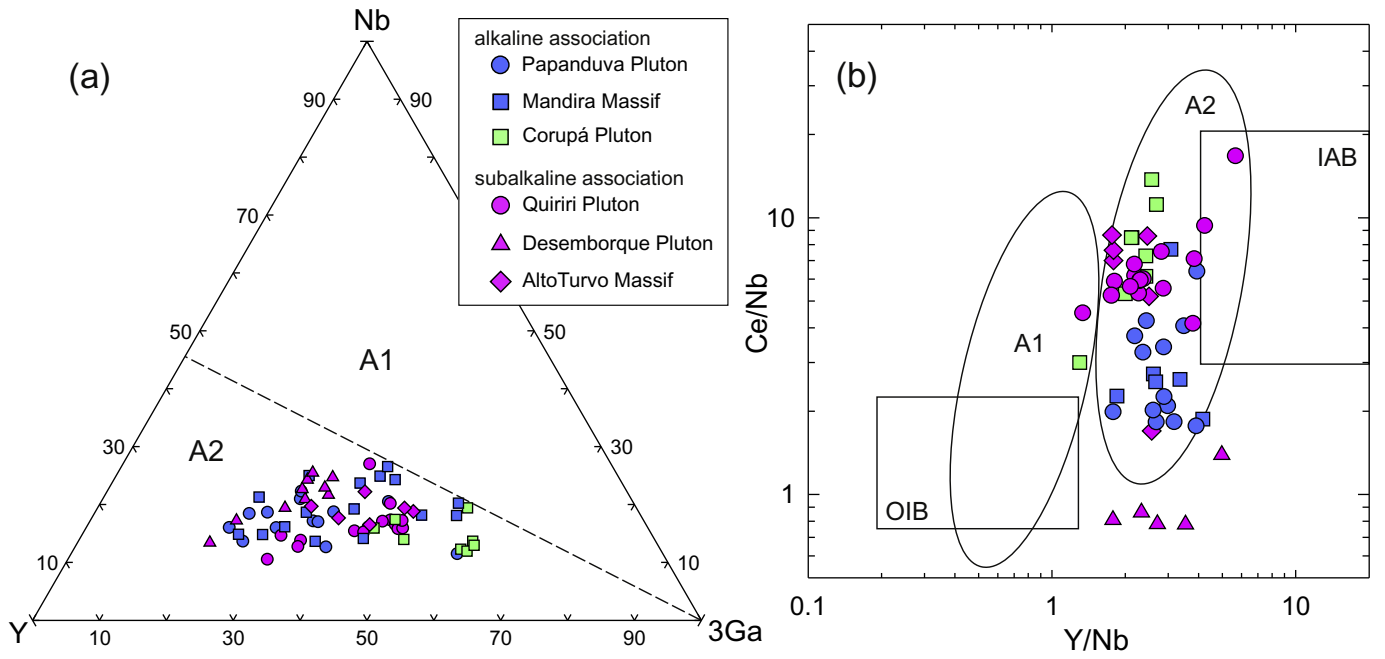

Fig. 2. Discrimination diagrams for A-type granitoids (Eby, 1990, 1992). (a) Ternary plot Nb – Y – 3*Ga (in ppm) to discriminate between A1 and A2-type granitoids. The dashed line corresponds to Y/Nb ratio of 1.2 (Eby, 1992). (b) binary plot Y/Nb vs. Ce/Nb ratios. Fields represent A1- and A2-type granites of Eby (1990). OIB: oceanic island basalt; IAB: island arc basalt. Data from Vilalva and Vlach (2014), Vlach and Gualda (2007), and our unpublished data.

amphiboles. This is the most common rock type within the pluton. Sample CO-32C corresponds to an oversaturated (SiO_2 = 61.9 wt%), green-colored, leucocratic (5 < M' < 15) quartz alkali feldspar syenite with hedenbergite, sodic to sodic-calcic amphiboles, and fayalite. Sample CO-32D is a saturated (SiO_2 = 50.0 wt%), melanocratic (M' > 50) alkali feldspar syenite with hedenbergite, fayalite and biotite as the main mafic phases. Significant amounts of magnetite, along with olivine and clinopyroxene, occur locally as centimetric layers with cumulate textures intercalated with the green syenite (e.g. sample CO-32C). Zircon, chevkinite, ilmenite, and apatite are the accessory minerals (Garin et al., 2003). These rocks have a ferroan character (0.85 < Fe* < 0.97) and metaluminous to slightly peralkaline affinity, with 0.61 < A/CNK < 0.87, and 0.97 < A/NK < 1.13.

3.2. Subalkaline association

Samples MR-161 and MR-186A from the Quiriri Pluton correspond to massive, holo- to leucocratic (4 < M' < 7), pink-colored, medium-grained biotite syenogranites with ferroan (0.89 < Fe* < 0.90) and slightly peraluminous signature (A/CNK ~1.04; 1.11 < A/NK < 1.13). Zircon, magnetite, titanite, fluorite, and allanite are common accessory minerals. Chlorite and epidote are important hydrothermal, secondary minerals after biotite, especially in sample MR-161. Xenoliths of country rocks are locally found (Vilalva and Vlach, 2014).

Sample GUA-16 from the Desemborque Pluton is a massive, leucocratic (M'~7), white to light-pink, fine- to medium-grained biotite alkali feldspar granite with slightly metaluminous signature (A/CNK = 0.98; A/NK = 1.05). Ilmenite, zircon, fluorite, and some sphalerite and topaz are the accessory minerals. Of note, the Desemborque Pluton is characterized by the highest values for the Fe* number within the subalkaline association (~0.99), similar to those found in the alkaline association (Garcia, 2015).

The Alto Turvo Massif sample (AT-15C) is a massive, leucocratic (6 < M' < 7), light-pink, coarse-grained biotite monzogranite showing ferroan character (Fe* = 0.83), and slightly metaluminous signature (A/CNK = 0.98; A/NK = 1.2). Accessory minerals are titanite, apatite, zircon, magnetite, and ilmenite (Vogado et al., 2011).

4. Analytical methods

4.1. Zircon selection

Fractions of ~25–50 euhedral zircon crystals and crystal fragments were obtained from 3 to 5 kg for each sample following the procedures described in Vlach et al. (2011). Cathodoluminescence (CL) and secondary electron (SE) imaging guided the selection of areas for in situ U-Pb dating, Hf isotope and trace element measurements. U-Pb, Hf and O isotope analysis were carried out at the MITERAC and CEST facilities, University of Notre Dame, USA. Trace element abundances were measured at the GeoAnalítica-USP facility, Geosciences Institute, University of São Paulo, Brazil.

4.2. U-Pb dating

In-situ LA-ICP-MS U-Pb age determinations were conducted on zircon crystals using a Thermo-Finningan Element2 ICP-MS instrument coupled to a nanosecond New Wave Research UP-213 laser ablation system. Ablation experiments were performed with a 30 μm laser spot diameter, 4 Hz repetition rate, and energy fluence of ~4–5 J/cm^2. Total acquisition time was 75 s, with 30 s for background measurement followed by 30 s of laser ablation data acquisition, and 15 s of washout time, following Frei and Gerdes (2009) and Simonetti and Neal (2010). The acquired ion signals were: ^{202}Hg, ^{204}(Pb + Hg), ^{206}Pb, ^{207}Pb, ^{208}Pb, ^{232}Th, ^{235}U, and ^{238}U. ^{202}Hg was measured to monitor the ^{204}Hg interference on ^{204}Pb. The method does not include a common Pb correction. However, individual measurement scans that recorded ^{204}Pb cps subsequent to the ^{204}Hg correction (based on the ^{202}Hg ion signal) were simply rejected (Simonetti and Neal, 2010). Correction for laser induced elemental fractionation (LIEF) was carried out by repeated analysis of the zircon standard BR-266 (Stern and Amelin, 2003) after 15 unknown measurements. Data reduction, including propagation of analytical uncertainties, followed procedures outlined in detail in Simonetti et al. (2005) and Simonetti and Neal (2010). The *Isoplot* software (Ludwig, 2012) was used for data reduction and plotting purposes.

4.3. LA-ICP-MS trace element analyses

In-situ zircon trace element abundances were quantified using an Elan 6100DRC ICP-MS instrument coupled to a nanosecond New Wave Research UP-213 laser ablation system. The measurements were carried out on the same dated crystals using a laser spot of 30 μm, 4 Hz repetition rate, and energy fluence of ~10 J/cm^2. Total acquisition time was 120 s, equally divided between background and laser ablation ion signals. The NIST SRM 612 glass wafer was employed as the external calibration standard, while an averaged SiO_2 abundance of 31.6 wt% (S.R.F. Vlach, unpublished data), was chosen as the internal standard. The *Glitter* software (van Achterbergh et al., 2001) was used for drift correction, data reduction and elemental abundance determinations.

4.4. Hf isotopes

The same zircon grains that were investigated for their U-Pb ages were also analyzed for in-situ Hf isotope composition. The analyses were conducted with a NWR193nm Excimer laser ablation system (New Wave Research) coupled to a NuPlasma II multicollector MC-ICP-MS (Nu Instruments). The grains were ablated using a 50 μm spot size, 10 Hz repetition rate, laser output corresponding to a fluence of ~14 J/cm^2, and He flow rate (within the laser ablation cell) of ~0.20 L/min. The following ion signals were simultaneously acquired: ^{171}Yb, ^{172}Yb, ^{173}Yb, ^{175}Lu, ^{176}Hf, ^{177}Hf, ^{178}Hf, ^{179}Hf and ^{180}Hf. Isobaric interference corrections for ^{176}Lu and ^{176}Yb on ^{176}Hf, using the exponential law, assumed that the instrumental mass bias for Lu = Yb = Hf (as discussed in Pearson et al., 2008). Each analysis consisted of 45 s baseline measurement followed by a laser ablation interval that lasted between 45 and 100 s. The external reproducibility and validation of the analytical protocol was evaluated by repeated analysis of the Mud Tank (n = 19) and 91,500 (n = 10) zircon standards during our measurements. They yielded average ^{176}Hf/^{177}Hf values of 0.28248 ± 0.00006 (2σ) and 0.28228 ± 0.00002 (2σ), in close agreement with the accepted ^{176}Hf/^{177}Hf values of 0.282504 ± 0.000044 (2σ, Woodhead and Hergt, 2005) and 0.282308 ± 0.000006 (2σ, Blichert-Toft, 2008), respectively.

4.5. Oxygen isotopes

In-situ oxygen isotope ratios for individual zircon separates of ~0.6 to 3.0 mg, collected after careful picking under a stereomicroscope, were obtained using a ESI-New Wave Research MIR-10 laser fluorination system, coupled to a silicate extraction line (method after Sharp, 1990), and measured using a Thermo Fisher Scientific Delta V Plus mass spectrometer. Instrumental fractionation of the ^{18}O/^{16}O isotope ratios was monitored via repeated analysis of the synthetic Lausanne Quartz standard (certified ^{18}O/^{16}O value = 18.15‰; Jourdan et al., 2009) using a "sample-standard" bracketing technique during each analytical session.

5. Results

5.1. Zircon crystal morphology and U-Pb dating

Fig. 3 shows representative zircon crystals from the studied samples along with the location of spots for U-Pb, trace element and Hf isotope analyses. The U-Pb data are listed in Supplementary Table 1.

5.1.1. Alkaline association

Zircon in the peralkaline granites (Papanduva Pluton and Mandira Massif) occurs as subhedral to euhedral grains (100 to 300 μm along the c crystallographic axis) with well-developed {100}-prism and {101}-pyramid surfaces, as typical for zircon from alkaline series granites (Pupin, 1980). CL imaging reveals concentric oscillatory to sectorial ("hour-glass") zoning and internal features indicating imprints of subsolidus, hydrothermal reactions (Fig. 3; Corfu et al., 2003). Zircon crystals in the syenites (Corupá Pluton) are divided into two morphological groups identified as Zrn1 and Zrn2 (Fig. 3). Crystals from the Zrn1 group are large (>300 μm long) blocky grains with well-developed {101}-pyramid and weakly developed {110}-prism faces. CL images depict an incipient to broad banded zoning with weak to moderate CL brightness. These large grains occur in the green syenite (sample CO-32C) and in the melasyenite (sample CO-32D). Zrn2 group is made up of subhedral to euhedral crystals (140–300 μm long) with well-developed {100} and {101} faces. They occur in the pink syenite (CO-38) and as a distinct textural generation in the melasyenite (CO-32D). Most crystal cores have indistinct, concentric, and sectorial zoning with weak CL brightness, as well as embayment due to local reabsorption. Their rim zones show a narrow concentric oscillatory zoning.

Age results for the Papanduva Pluton and Mandira Massif are shown in Fig. 4. Individual analyses for the Papanduva Pluton (Fig. 4a) are associated with elevated discordances probably due to Pb loss, and at least two age populations are recognized. Application of the deconvolution method of Sambridge and Compston (1994) resulted in a two-component split of the zircon population (Fig. 4a) at 557 ± 10 Ma (31% of the whole population), and 578 ± 6 Ma (69% of population). Weighted mean (WM) ^{206}Pb/^{238}U ages of both populations are 554 ± 8 Ma (n = 7; MSWD = 0.28), and 580 ± 5 Ma (n = 15; MSWD = 0.42), respectively; the latter is interpreted as the most reliable estimate for the crystallization age. Of note, it appears that there is no correlation between age populations and location of laser ablation spot within the analyzed zircon crystals.

For the Mandira Massif (Fig. 4b), ten analytical spots (with >80% concordance) resulted in a WM ^{206}Pb/^{238}U age of 567 ± 6 Ma (MSWD = 0.29), which overlaps (within errors) the younger age population recorded in the Papanduva Pluton.

Fig. 4c–e show the age results for the Corupá syenites. For the pink syenite (Fig. 4c), twenty-three analyzed spots (with >76% concordance) yielded a WM ^{206}Pb/^{238}U age of 576 ± 5 Ma (MSWD = 1.0). For the green syenite (Fig. 4d), fourteen out of twenty-four analyses, all within 10% discordance, yield a concordant age of 583 ± 5 Ma (MSWD = 1.13). Seventeen analyzed data points for the melasyenite (Fig. 4e) with degrees of discordance <10% resulted in a concordant age of 577 ± 4 Ma (MSWD = 2.6).

5.1.2. Subalkaline association

Zircon grains from the peraluminous and metaluminous granites of the Quiriri and Desemborque Plutons, and Alto Turvo Massif show a variety of habits (Fig. 3). Most grains are euhedral, 70 to 300 μm long, with moderate developed {110}-prism and well-developed {101}-pyramid faces. The predominance of the prismatic {110} form increases from the Quiriri Pluton to Alto Turvo Massif and Desemborque Pluton. The remainder grains are stubby, with moderate to well-developed {100}-prism and weak developed {211}-pyramid faces. CL images reveal ubiquitous zoning and some complex internal textures. Partial dissolution, local resorption and recrystallization, hydrothermal overgrowths, similar to those described by Corfu et al. (2003), as well as the occurrence of inherited components and inclusions are common features in zircon from the Alto Turvo Massif and Desemborque Pluton (Fig. 3).

U-Pb age results for the Quiriri and Desemborque Plutons, and Alto Turvo Massif are given in Fig. 5. For the Quiriri Pluton, the deconvolution method of Sambridge and Compston (1994) revealed two populations in sample MR-161 (Fig. 5a) at 539 ± 7 Ma (35% of the whole population), and 580 ± 6 Ma (65% of population). WM ^{206}Pb/^{238}U ages are 540 ± 9 Ma (n = 9; MSWD = 1.6), and 580 ± 5 Ma (n = 17; MSWD = 0.98), respectively (Fig. 5a); the latter is interpreted as the crystallization age. Analyses yielding younger ages come from both zircon rims and cores. In sample MR-186A (Fig. 5b), nineteen spots with discordances <10% yield a concordant crystallization age of 578 ± 4 Ma (MSWD = 0.04). Excluding the ~540 Ma population, the entire

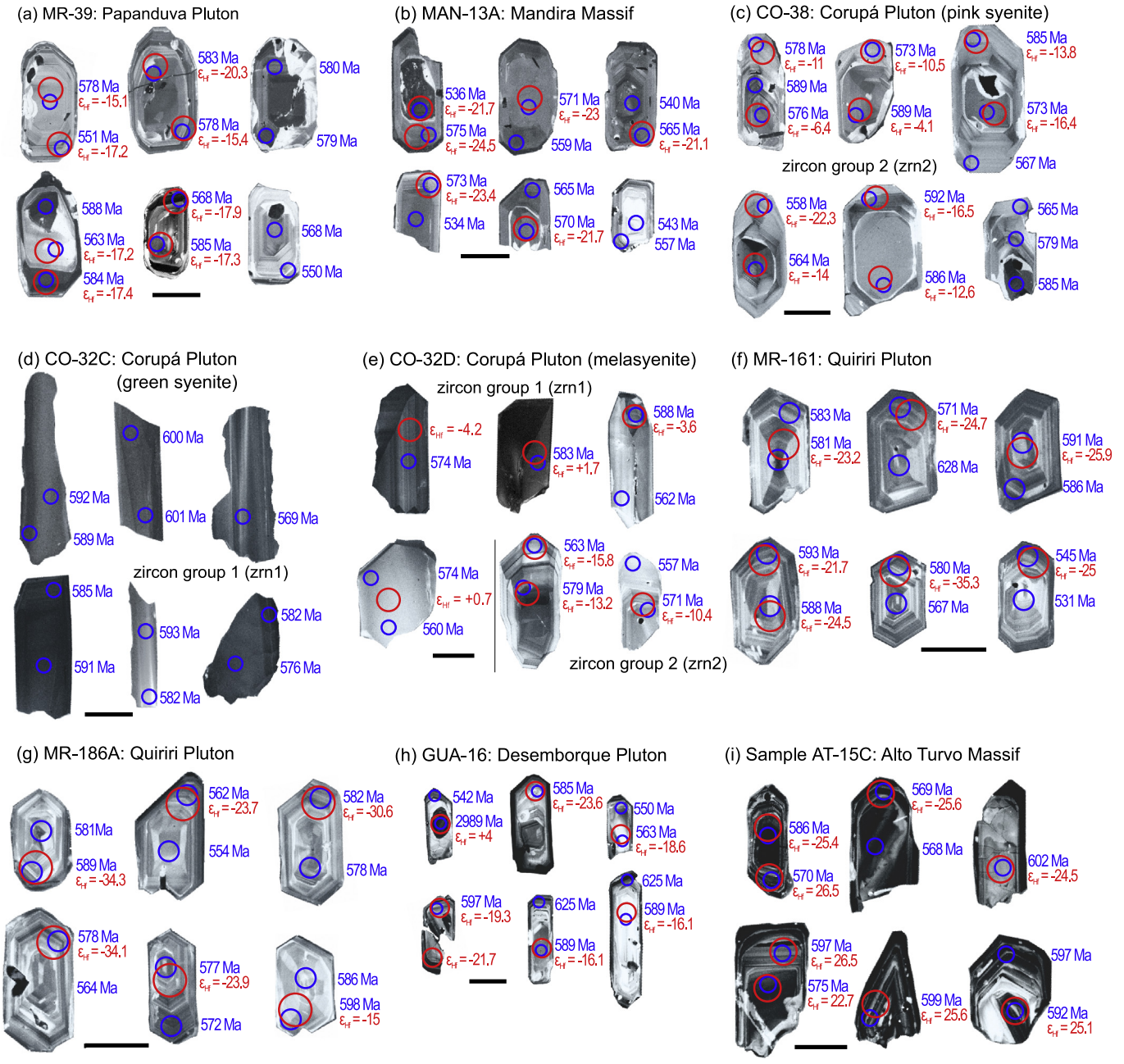

Fig. 3. Cathodoluminescence (CL) images of representative zircon crystals from the studied alkaline and subalkaline granitic and syenitic plutons from the A-type Graciosa Province, with the location of U-Pb and Lu-Hf analytical spots. Scale bar = 100 μm.

data set for samples MR-161 and MR-186A is a statistically coherent cluster with a WM $^{206}Pb/^{238}U$ age of 578 ± 3 Ma (n = 43; MSWD = 1.08), considered the best estimate for the crystallization age of the Quiriri Pluton (Fig. 5c).

Sample GUA-16 from the Desemborque Pluton yielded a WM $^{206}Pb/^{238}U$ crystallization age of 580 ± 8 Ma (n = 9; MSWD = 0.92; Fig. 4d). Concordant age determinations are difficult to obtain due to the common presence of inheritance (mainly between 620 and 700 Ma), and to the strong late-stage hydrothermal imprint that affected many of the primary zircons within this pluton (Garcia, 2015). Nevertheless, this was the only investigated granite to record an older, Archean inheritance of ~3.0 Ga, obtained within a single zircon core. This finding combined with the age result of ~580 Ma (discordances <10%) leads to a discordia with a lower intercept of 581 ± 12 Ma, and an upper intercept age of 2.97 ± 0.023 Ga (MSWD = 0.80), calculated using a Monte Carlo statistical approach (Fig. 5d).

U-Pb age determinations for the Alto Turvo Massif (Fig. 5e) range from 568 to 602 Ma. Three analytical spots record older ages between 607 and 695 Ma, and these typically occur as cores within younger rims, indicating inheritance. Moreover, nine spots were excluded because of large $^{206}U/^{238}Pb$ age deviation or low degree of concordance (Pb loss). Thirteen remaining analyses yield a WM $^{206}Pb/^{238}U$ age of 584 ± 8 Ma (MSWD = 1.7). Among these, six analyses with associated degrees of discordance <13% result in a concordant age of 585 ± 7 Ma (MSWD = 1.08) (Fig. 5e).

5.2. Zircon chemistry and thermometry

Trace element abundances for the investigated zircon grains are given in Supplementary Table 2. Due to the presence of micro-inclusions of chevkinite, allanite, apatite and titanite, data presented herein has been screened and culled based on anomalously high P, Th, Ti associated with elevated light rare earth element (LREE) abundances.

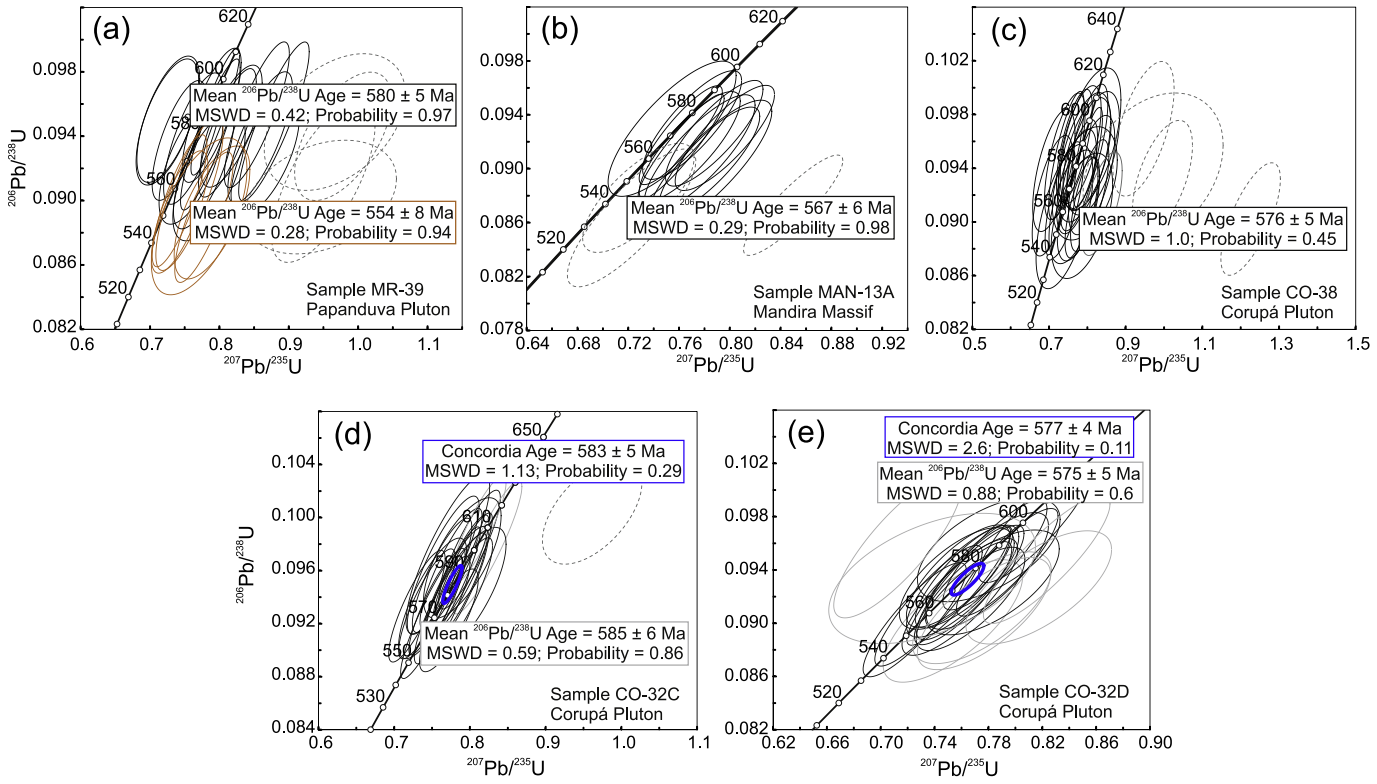

Fig. 4. Concordia diagrams for the alkaline granites and syenites samples of the A-type Graciosa Province. Data-point error ellipses are 2σ. Dashed ellipses are discordant data not included in calculations.

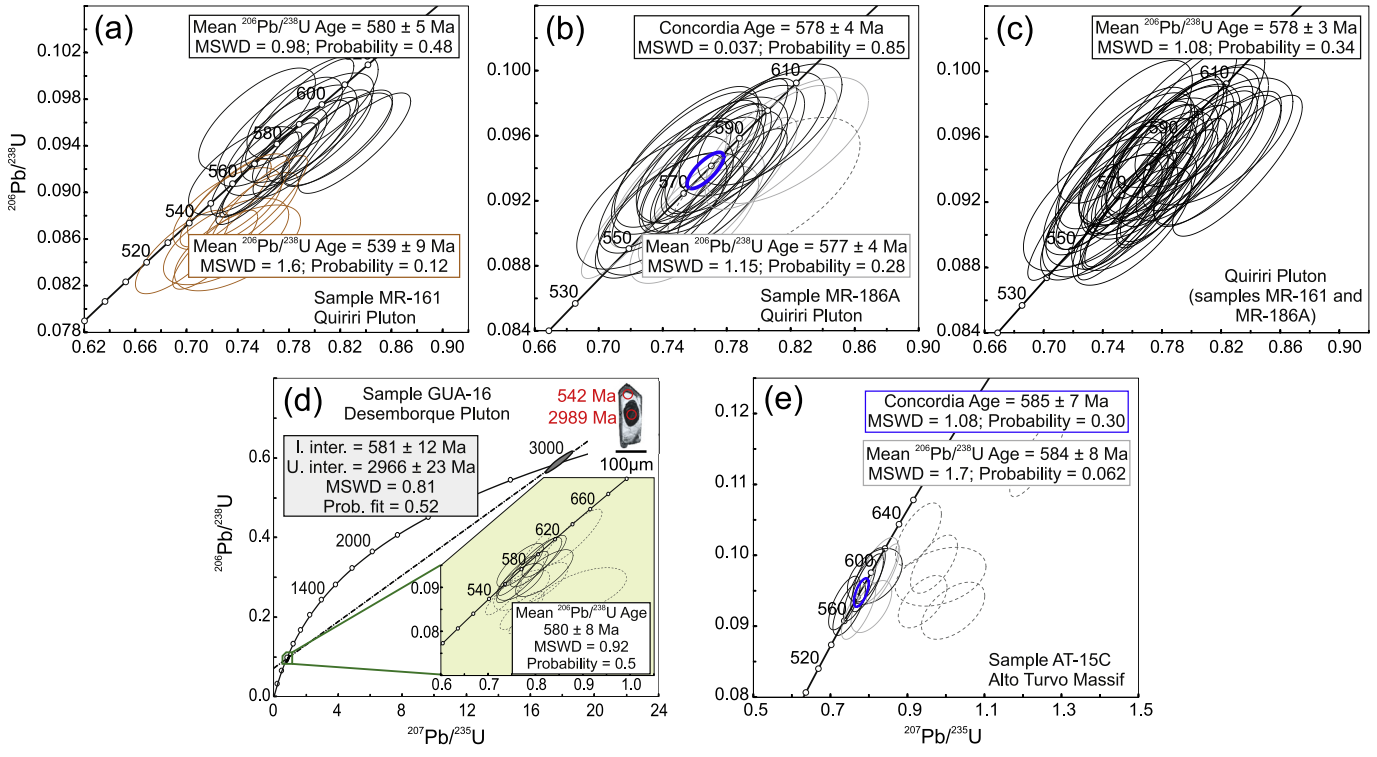

Fig. 5. Concordia diagrams for the subalkaline granites samples of the A-type Graciosa Province. Data-point error ellipses are 2σ. Dashed ellipses are discordant data not included in calculations.

In general, trace element contents correlate with CL intensities for different crystal zones. Those with high CL brightness (Fig. 3) correspond to high Nb, Hf and Zr contents (Fig. 6). Conversely, zones with low CL brightness (Fig. 3) have high Th and U contents (Figs. 6a–b). Ti and REE contents are variable. However, the relationship between CL intensity variations and crystal morphological

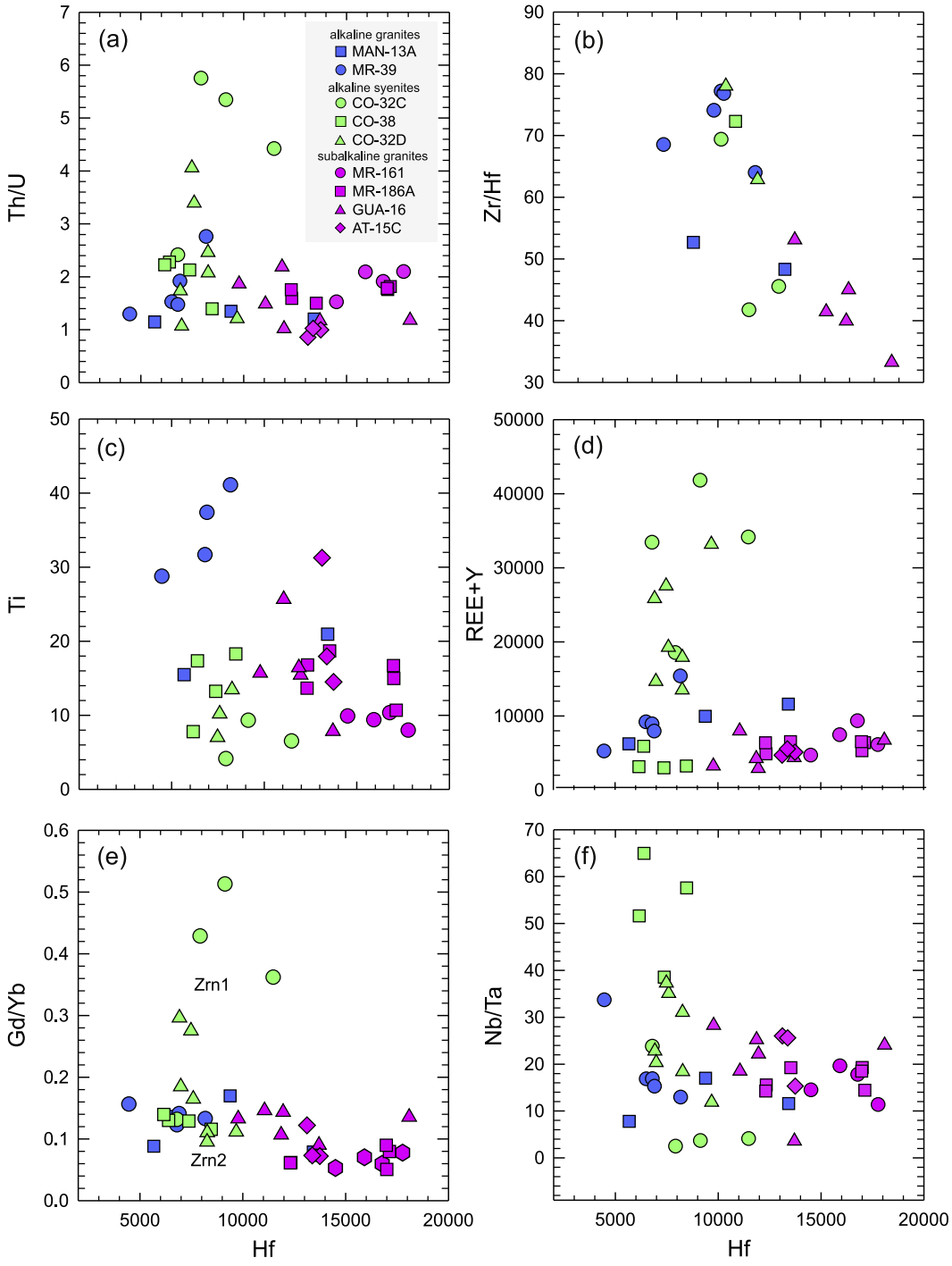

Fig. 6. Bivariate plots showing hafnium concentration (in ppm) and covariation trends with: (a) Th/U; (b) Zr/Hf; (c) Ti; (d) REE + Y; (e) Gd/Yb; and (f) Nb/Ta in zircon crystals from the studied granites and syenites of the A-type Graciosa Province.

positions (core, rim and intermediate position) is not always straightforward.

The analyzed zircon crystals are characterized by relatively high Th/U ratios, between 0.9 and 2.8, and up to 5.8 for those within the Corupá syenites (Fig. 6a), reflecting elevated Th abundances. According to Breiter et al. (2014), high contents of Th, Hf, Y and U (and thus Th/U), among other trace elements, are typical signatures of evolved A-type granites. Ti contents are higher in the Papanduva zircon crystals (29–41 ppm) and correlate positively with Hf (Fig. 6c).

Hafnium abundances can distinguish between zircon from subalkaline and alkaline associations (Fig. 6). Zircon crystals in the subalkaline granites have Hf contents > ca. 10,000 ppm, while in the alkaline granites and syenites their Hf abundances are < ca. 10,000 ppm. Among the Corupá syenites, the blocky Zrn1 crystals from samples CO-32C (green syenite) and CO-32D (melasyenite) are characterized by high Y, and REE contents, and Th/U and Gd/Yb ratios (Fig. 6a, d–e). Zrn2 crystals from sample CO-38 (pink syenite) have high Nb/Ta ratios (6f).

The chondrite-normalized REE patterns (Fig. 7) are typical of igneous zircon (e.g. Hoskin and Schaltegger, 2003). They show a rather steeply-rising slope due to HREE enrichment relative to LREE ($13 < Yb_N/Ce_N < 144$), and distinctive positive Ce and negative Eu anomalies, with Ce/Ce* [$Ce_N/(La_N{*}Pr_N)^{1/2}$] and Eu/Eu* [$Eu_N/(Sm_N{*}Gd_N)^{1/2}$] up to 81 and 1.0, respectively. Zircon in the Corupá syenites has the most contrasting REE compositions (Fig. 6d, Fig. 7b); crystals from the pink syenite have

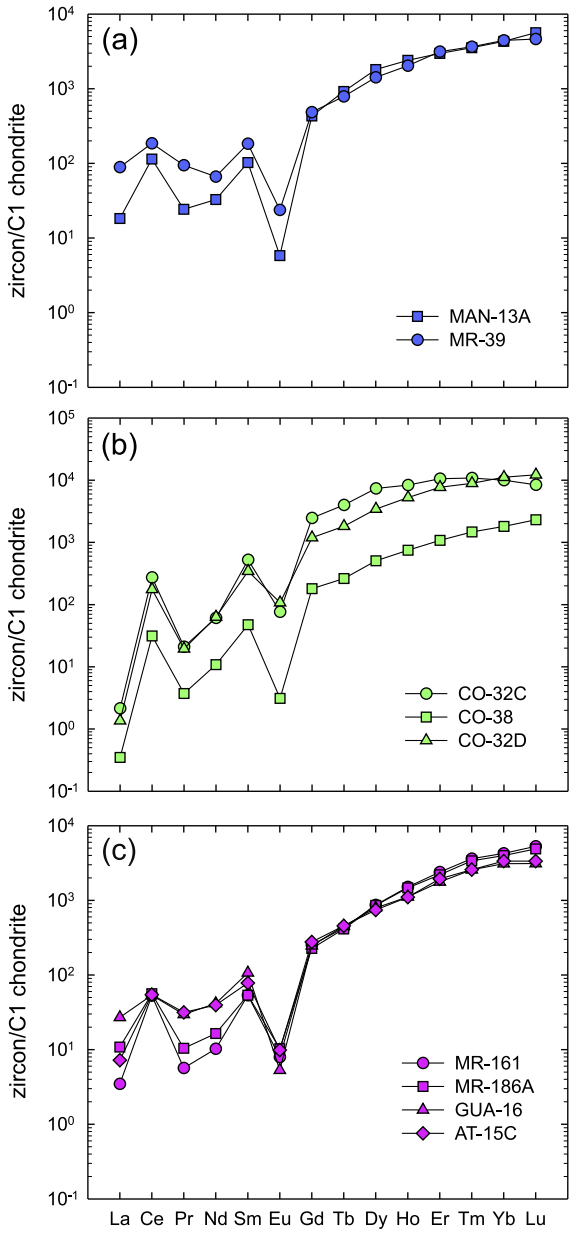

Fig. 7. Median chondrite-normalized rare-earth patterns for zircon crystals from the studied (a) alkaline granites, (b) syenites, and (c) subalkaline granites of the A-type Graciosa Province.

low REE contents (up to 2309 ppm; LREE up to 82; HREE up to 2227), whereas those from the green syenite and melasyenite are REE-rich (LREE up to 925 ppm; HREE up to 13,172). The Zrn2 in the melasyenite differs from the Zrn1 grains mainly in having higher Ce anomalies ($18 < Ce/Ce^* < 70$), and lower Gd/Yb ratios (≤0.11; Fig. 6e) reflecting slightly higher HREE contents. In peralkaline granites, zircon crystals show less apparent Ce anomalies (Ce/Ce^* up to 22) due to their high LREE contents (up to 553 ppm; Figs. 6a, 5h). In subalkaline granites (Fig. 7c), the zircon grains have REE abundances ranging from 1058 to 3803 ppm ($48 < LREE < 363$ ppm; $1003 < HREE < 3712$ ppm), and Ce anomalies are lower ($0.8 < Ce/Ce^* < 35$). Zircon grains from the Alto Turvo Massif and Desemborque Pluton display a relative LREE enrichment, with $(Sm/La)_N$ between 1.9 and 32.2 and 0.6–10.2, respectively (Fig. 6d, Fig. 7c).

5.2.1. Ti-in-zircon thermometry

The Ti-in-zircon geothermometer was used to estimate the magma temperature at the time of zircon crystallization (Ferry and Watson, 2007; Watson and Harrison, 2005). Calculations considered only Ti contents in accordance with the normal abundances in igneous zircon (Ti ≤ 75 ppm, Hoskin and Schaltegger, 2003). A value of 0.7 was assumed for the $aTiO_2$ (Clairbone et al., 2010), whereas the $aSiO_2$ was fixed at 1.0, except for the saturated syenite of sample CO-32D where $aSiO_2 = 0.9$.

Calculated Ti-in-zircon temperatures (T_{ZrTi}) are given in Supplementary Table 2. They are slightly higher and span over a wide range (826–945 °C) in the peralkaline granites. Mean temperatures are 921 ± 14 °C (Papanduva Pluton) and 843 ± 17 °C (Mandira Massif). Temperatures for the Corupá syenites vary from 699 to 845 °C (mean value of 777 ± 37 °C). The pink syenite has the highest values (mean value of 812 ± 30 °C); while the Zrn1 grains in the green syenite have the lowest calculated temperatures (mean value of 737 ± 26 °C). Calculated T_{ZrTi} for the melasyenite vary between 736 and 800 °C (mean value of 770 ± 22 °C). Within this petrographic facies, Zrn1 blocky grains crystallized at temperatures of 754 ± 18 °C, whereas the euhedral, high-CL Zrn2 crystals formed at 800 °C. Subalkaline granites are characterized by temperatures between 757 and 909 °C. The highest T_{ZrTi} values are found in the Alto Turvo Massif (857 ± 38 °C) and in the Desemborque Pluton (826 ± 41 °C). Zircons from the Quiriri Pluton crystallized at 804 ± 29 °C.

5.3. Hf and O isotope geochemistry

The Hf isotopic compositions are listed in Supplementary Table 3. The εHf(t) values and depleted mantle Hf model ages (T_{DM}) was calculated using a decay constant for ^{176}Lu of 1.867×10^{-11} yr^{-1} (Söderlund et al., 2004), $(^{176}Lu/^{177}Hf)_{CHUR}$ and $(^{176}Hf/^{177}Hf)_{CHUR}$ values of 0.0336 and 0.282785, respectively (Bouvier et al., 2008), a present-day $^{176}Hf/^{177}Hf$ value of 0.283250, and a $(^{176}Lu/^{177}Hf)_{DM}$ value of 0.0384 (Griffin et al., 2000). Zircon grains of the subalkaline granites show a large range of $^{176}Hf/^{177}Hf$ ratios from 0.281564 to 0.281980, and εHf (t) between −16.5 and − 31. Their two-stage Hf model ages are between 2.3 and 3.1 Ga. The inherited core from sample GUA-16 (Fig. 3) yields $\varepsilon_{Hf(t)}$ of +4 ($^{176}Hf/^{177}Hf = 0.281068$) and a corresponding Hf model age of 3.1 Ga. Grains of the peralkaline granites show variation of $^{176}Hf/^{177}Hf$ ratios from 0.281756 to 0.282027. Those from the Papanduva Pluton are more radiogenic, with $\varepsilon_{Hf(t)}$ values between −15 and −20 and two-stage Hf model ages between 2.2 and 2.5 Ga. In contrast, zircon grains from the Mandira Pluton have $\varepsilon_{Hf(t)}$ values around −21 and −25, and Hf model ages between 2.6 and 2.8 Ga. The syenite zircon grains exhibit the largest variation of $^{176}Hf/^{177}Hf$ ratios from 0.281962 to 0.282515. Those from the pink syenite (sample CO-38) have $\varepsilon_{Hf(t)}$ ranging from −4 to −17, and two-stage Hf model ages from 1.6 to 2.3 Ga. The two zircon generations (Zrn1 and Zrn2) in the melasyenite sample (CO-32D) have distinct Hf signatures. The Zrn1 grains have $\varepsilon_{Hf(t)}$ between +1.4 to −5 and Hf model ages ranging from 1.3 to 1.7 Ga. Conversely, euhedral Zrn2 grains have distinctly lower $\varepsilon_{Hf(t)}$ values from −11 to −13, with corresponding Hf model ages of 2.0 to 2.2 Ga.

Oxygen isotope compositions were measured in zircon concentrates from the Papanduva, Desemborque, and Quiriri plutons, and from the Alto Turvo Massif. Additional $\delta^{18}O$ values for the Graciosa granites, syenites and gabbroic rocks obtained by Valley et al. (2005) were also incorporated for further discussion. The dataset is presented in Supplementary Table 4 and Fig. 8.

$\delta^{18}O$ in-zircon for the studied rocks lie mainly between 4.7 and 6.0‰, and are close to the accepted values for zircon in equilibrium with pristine mantle melts (5.3 ± 0.6‰; 2σ, Valley et al., 1998). These values are also similar to the average zircon $\delta^{18}O$ values obtained for country rocks of Curitiba (5.3 ± 0.9‰) and Luis Alves (5.6 ± 0.4‰) microplates (Valley et al., 2005). Granites from the alkaline and subalkaline associations have similar average $\delta^{18}O$ values of 5.6 ± 0.2‰ (n = 4) and 5.8 ± 1.0‰ (n = 12), respectively (Fig. 8). The largest deviation for the subalkaline granites is due to the enriched $\delta^{18}O$ values of 2.7 to

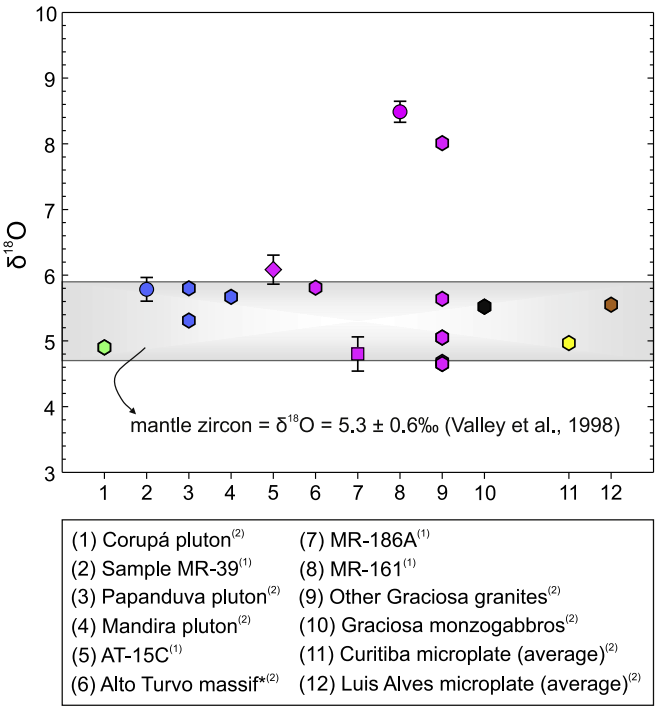

Fig. 8. Oxygen isotope composition of zircons from the A-type granitoids and associated rocks, and from the basement rocks of the Graciosa Province. *: monzonite. Data source: (1) this work; (2) Valley et al. (2005).

3.2‰ relative to pristine mantle values found in sample MR-161 ($\delta^{18}O = 8.5 \pm 0.2‰$; this work), and in the Serra do Paratiú/Cordeiro Pluton ($\delta^{18}O = 8.0‰$; Valley et al., 2005). According to Valley et al. (2005), the Corupá pink syenites have zircon $\delta^{18}O = 4.9‰$.

6. Discussion

6.1. Geochronological overview

Vlach et al. (2011) reviewed the available geochronological data for the Graciosa Province. The compilation of reliable K-Ar (biotite and amphibole), Rb-Sr (whole-rock), and U-Pb (ID-TIMS, SHIRMP) age determinations yielded weighted means (WM) of 576 ± 26 Ma, 580 ± 20 Ma and 581 ± 16 Ma, respectively. These authors also obtained new zircon ID-TIMS ages for coeval and mingled gabbro-dioritic rocks, whose zircon crystals were less prone to present inheritance and/or post-magmatic overprints, as compared to granites and syenites. Based on their concordant results, Vlach et al. (2011) suggested 580–583 (±3) Ma as the best reference crystallization age for the whole province. The authors also pointed out that the overall agreement among those chronometers is consistent with magma emplacement at shallow levels, under relatively fast cooling rates.

Our expanded results yield a well-constrained WM $^{206}Pb/^{238}U$ age of 579 ± 5 Ma (MSWD = 0.58; Fig. 9) and strongly agree with Vlach et al. (2011). On the other hand, given our extended sampling, the data presented here put a better upper limit to the time span among alkaline and subalkaline/aluminous intrusions emplacement, evolution and crystallization in an interval <9 Ma, with similar peak magmatism at ~580 Ma. In this context, the Mandira Massif, at the northeastern area of the province, represents the latest episode of this A-type magmatism. Arguably, this may suggest a fast-magmatic focus migration within the province, propagating in a southwest to northeast direction. Lastly, our results corroborate the synchronicity between the Graciosa and Itu A-type Provinces, as suggested by Vlach et al. (2011), the latter located to the north of the studied area, within the Apiaí-Guaxupé Terrain (Janasi et al., 2009; Fig. 1).

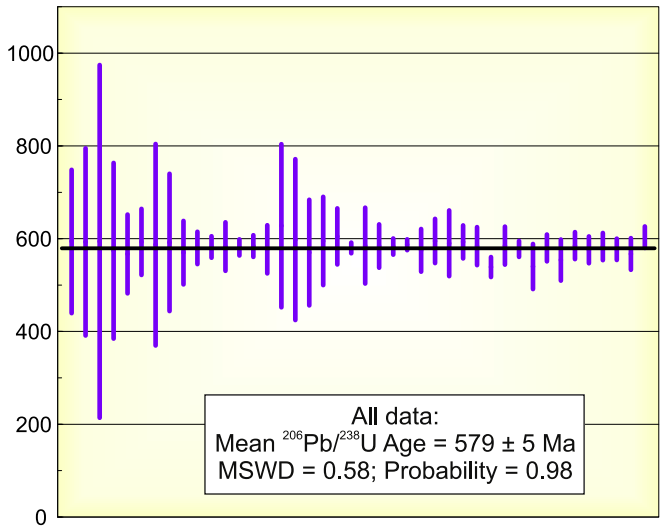

Fig. 9. Weighted average $^{206}Pb/^{238}U$ age diagram obtained for all available geochronological data for the A-type Graciosa Province, including new data here obtained. The age represents the climax for the Graciosa magmatism.

6.2. On the LREE enrichment in zircon

Many zircon crystals from the peralkaline granites, the syenites of samples CO-32C and CO-32D, and from the subalkaline Desemborque Pluton, exhibit variable LREE enrichment, that can be monitored based on the $(Sm/La)_N$ ratio (Hoskin, 2005; Fig. 10). The most common explanation for LREE enrichment in zircon is accidental sampling of LREE-bearing mineral inclusions, such as chevkinite, allanite, titanite or apatite. We believe that monitoring of P, Th, and Ti ion signals within the time-resolved spectrums during ablation experiments helps to identify and eliminate the presence of inclusions and therefore rules out such an explanation. However, it is still possible that zircon contains sub-microscopic inclusions that are hard to detect and could lead to an overestimate of LREE.

High LREE contents can also be attributed to zircon alteration by LREE/HFSE-enriched late hydrothermal fluids, or even its direct precipitation from these fluids. In fact, the circulation of F- and HFSE-rich

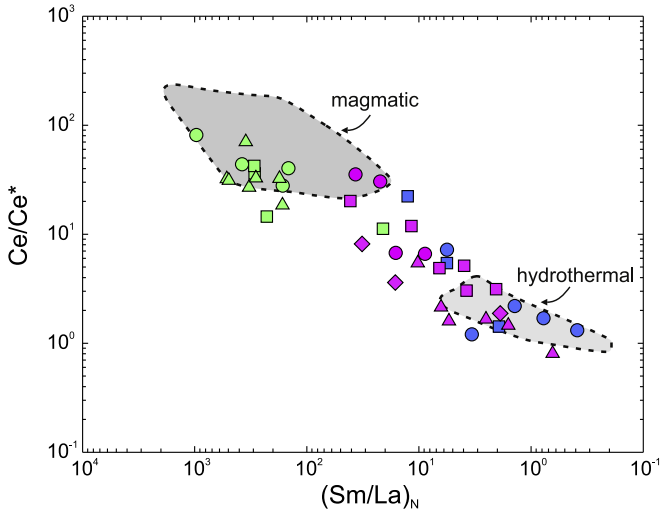

Fig. 10. $(Sm/La)_N$ versus Ce/Ce* bivariate discriminant plot of magmatic and hydrothermal zircon for the analyzed zircon crystals from the A-type Graciosa Province. Fields of "magmatic" and "hydrothermal" from the Boggy Plain Zoned Pluton, Australia (Hoskin, 2005). Symbols as in Fig. 6.

residual fluids under relatively oxidizing conditions leading to the formation of REE-bearing hydrothermal minerals (e.g. epidote, allanite), or promoting intense re-equilibration of primary REE-bearing minerals (e.g. chevkinite) is a well-known phenomenon within the province (Vlach, 2012; Vlach and Gualda, 2007). Zircon found in the syenites falls within or near the magmatic field in Fig. 10, whereas zircon from the subalkaline plutons has compositions intermediate between typical magmatic and hydrothermal, but trend towards hydrothermal signatures (e.g. some crystals from the Quiriri Pluton). Zircon from the subalkaline Desemborque Pluton and from the peralkaline granites plot mainly inside the hydrothermal field (Fig. 10). They show flatter LREE patterns (Fig. 7a) as expected for zircon that has re-equilibrated with hydrothermal fluids (e.g. Hoskin, 2005). Accordingly, metamict crystals and/or hydrothermal overgrowths with high LREE and weak CL contrast are relatively common in the Mandira Pluton, whereas dissolution/re-precipitation textures are widespread in zircons from the Papanduva Pluton (Fig. 3). In the latter, zircon is also intergrown with late- to post-magmatic albite laths (Vilalva and Vlach, 2014). These crystals have precipitated from LREE-enriched melts, since LREEs would be more incompatible than HREEs.

The recognition of hydrothermal overprint in zircon based solely on REE contents is not straightforward (Cavosie et al., 2006). For example, Fu et al. (2009) showed that true hydrothermal zircons contain indistinguishable chemical and isotopic compositions relative to their magmatic counterparts. For the Corupá syenites, zircon grains from samples CO-32C and CO-32D have typical magmatic compositions (Fig. 10); nevertheless, they show relatively high contents of some LREEs (e.g. Pr, Sm), as well as yttrium. In fact, the Zrn1 zircon grains from samples CO-32C and CO-32D (Fig. 3) have the most contrasting morphology and chemical characteristics among the analyzed crystals. Their unusually high Th/U ratios (Fig. 6a) are due to elevated abundances of both Th and U rather than reflecting the co-precipitation of other U- and/or Th-bearing minerals (e.g. thorite, monazite). Furthermore, crystallization ages are slightly older within their associated uncertainties, and the Ti-in-zircon temperatures are lower when compared to the zircon crystals from the pink syenite (Fig. 4c–e). We suggest that these crystals are potential antecrysts: i.e., zircon that crystallized from an earlier, less fractionated, pulse of magma and was incorporated in a later pulse (cf. Miller et al., 2007) from which euhedral zircon in sample CO-32D and in the main pink syenite (sample CO-38) precipitated.

6.3. Oxidation states and temperatures in the zircon crystallizing environments

Partitioning of Ce^{4+} into the zircon structure is favored relative to Ce^{3+} and the proportion of Ce^{3+} relative to Ce^{4+} is a function of the fO_2. Therefore, the Ce^{4+}/Ce^{3+} ratio in zircon acts as a proxy of magma oxidation state (Ballard et al., 2002; Trail et al., 2012). The calculation of Ce^{4+}/Ce^{3+} ratio according to the method of Ballard et al. (2002) requires trace element and REE contents of the zircon and its host rock. Among the studied samples, complete whole-rock compositions are available for samples MR-39 (alkaline association), and MR-161 and MR-186A (subalkaline association) (Vilalva and Vlach, 2014). The calculated zircon Ce^{4+}/Ce^{3+} ratios for these samples vary from 1.6 to 103.1. Among these, the Ce^{4+}/Ce^{3+} values for the subalkaline granites (5.5–103.1; average = 37.4) are higher than those for the peralkaline granite (1.6–35.5; average = 16.7), suggesting a crystallization under slightly more reduced conditions for the latter. These results corroborate with textural and mineralogical evidences that qualitatively suggest crystallization conditions close to the FQM (fayalite – quartz – magnetite) buffer for the granites and syenites of the alkaline association, and close to (or higher than) the TMQAI (titanite – magnetite – quartz – amphibole – ilmenite) buffer for the subalkaline granites (e.g. Garin et al., 2003; Gualda and Vlach, 2007a; Vilalva and Vlach, 2014).

The calculated Ti-in-zircon temperatures for the syenites and subalkaline granites are coherent with experimental data for A-type rocks (Scaillet et al., 2016; Turner et al., 1992), and with zircon saturation temperatures for the Graciosa Province (750–900 °C; Gualda and Vlach, 2007a). The higher temperatures found mainly in the Alto Turvo Massif and Desemborque Pluton may reflect the presence of inherited crystals, as corroborated by the geochronological data (see Section 5.1.2; cf. Siégel et al., 2018). For the peralkaline granites, Ti-in-zircon temperatures are too high (especially for the Papanduva Pluton) and appear to be in disagreement with experimental constraints from peralkaline volcanic systems (Scaillet et al., 2016). These overestimated temperatures may be related to inappropriate calibrations (especially aTiO2) for these particular systems (Watson and Harrison, 2005).

6.4. Petrogenetic implications

Petrogenetic models for A-type granites are still a matter of debate (Bonin, 2007; Frost and Frost, 2011). There are three major petrogenetic pathways: (1) fractionation from mantle-derived magmas (Eby, 1990; Turner et al., 1992); (2) partial melting of crustal sources, mainly lower (granulitic) crust (Collins et al., 1982; Patiño-Douce, 1997; Whalen et al., 1987); and (3) mixing between crustal melts and mantle-derived mafic magmas (Yang et al., 2006). Recently, petrogenetic models involving A-type magma generation through partial melting of either metasomatized lower crust or lithospheric mantle (e.g., Jiang et al., 2018; Martin, 2006) have gained more attention. Both hypotheses would occur in an extensional setting involving lithospheric thinning, delamination, and asthenosphere upwelling.

Several investigations have demonstrated that the zircon Hf abundance increases with magmatic differentiation (e.g. Breiter et al., 2014; Hoskin and Schaltegger, 2003). Hence, the higher Hf abundances in zircon from the subalkaline granites suggest these rocks have crystallized from more differentiated melts than those giving rise to the alkaline granites and syenites. Nevertheless, partitioning of Hf into zircon has also been influenced by the co-crystallization of other HFSE-rich accessory minerals, as observed in the alkaline rocks.

Grimes et al. (2007, 2015) used U and Yb contents to discriminate between zircon crystallized from mantle sources and continental settings. Based on a large trace element database for zircon from different tectonic settings, these authors defined a reference “mantle-zircon array” in the bivariate plot U/Yb versus Nb/Yb (Fig. 11a). Compositions that fall above this field define a “magmatic arc array”. Fig. 11a reveals that zircon from both the alkaline and subalkaline rocks plot along the mantle-zircon array. Of note, these authors argued that zircon with high (>0.1) U/Yb values reflect either higher crustal (LIL-enriched) input in the parental melts, or an enriched mantle source.

Grimes et al. (2015) have also used the Gd/Yb ratio in zircon as a proxy for melt-source enrichment, as this ratio measures the MREE enrichment relative to HREE depletion, which is indicative of a “garnet signature” imposed on the parental melt when garnet is maintained as a residual phase in the enriched mantle source. Compositions for the Graciosa zircons are plotted in the binary Ce/Yb versus Gd/Yb diagram (Fig. 11b). Crystals herein interpreted as autocrysts from samples CO-32C and CO-32D define a distinct trajectory of enrichment in LREEs and MREEs relative to HREEs that is indicative of a “garnet signature” and, thus, suggesting the participation of enriched mantle sources. Crystals from the subalkaline granites show increasing Ce/Yb parallel to decreasing Gd/Yb ratios (in a direction orthogonal to the garnet signature); in contrast, the remaining crystals exhibit a general trend of concomitant decrease in Ce/Yb and Gd/Yb ratios, which is a direction opposite that expected from the garnet signature (Fig. 11b). These features reflect both zircon crystallization and fractionation of LREE and MREE-bearing accessory minerals. Alternatively, chemical signatures found in zircon crystals from the subalkaline granites, along with their high U/Yb ratios may reflect relatively high fractions of crustal contamination.

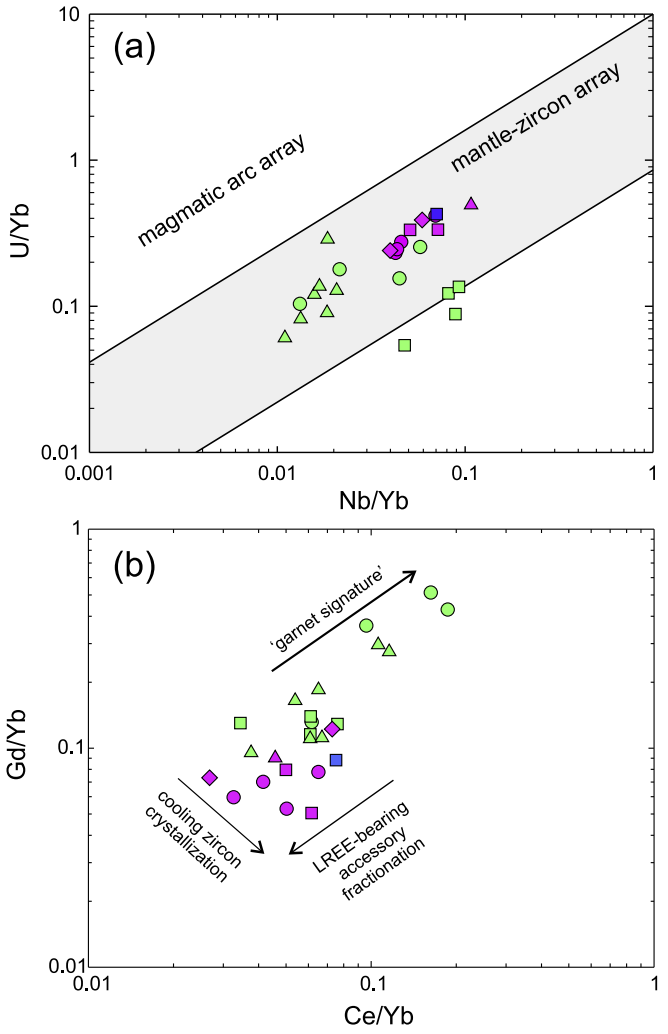

Fig. 11. Discrimination bivariate diagrams of Grimes et al. (2015) for zircon grains from the Graciosa A-type granites and syenites. (a) Nb/Yb versus U/Yb plot as a proxy for tectono-magmatic source of igneous zircon. (b) Bivariate Ce/Yb versus Gd/Yb plot emphasizing the presence of a "garnet signature" that points to the presence of enriched mantle source in the generation of the syenites from the A-type Graciosa Province. The plot also depicts the influence of LREE-bearing accessory fractionation and zircon crystallization on the trace element ratios. Compositions for LREE-rich zircon crystals from Desemborque and Papanduva Plutons, and the Mandira Massif (except for one sample) were excluded so as to avoid samples affected by post-magmatic geochemical overprints. Symbols as in Fig. 6.

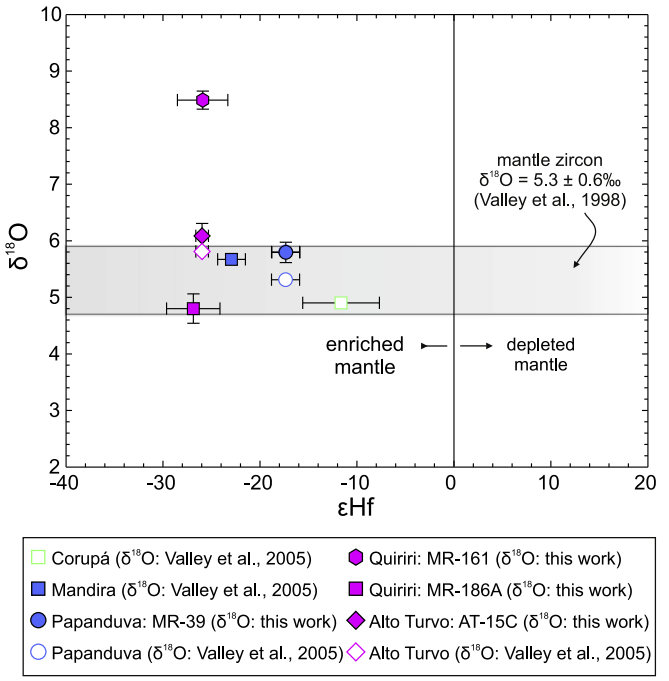

Fig. 12. Binary plot ε_{Hf} vs $\delta^{18}O$ for zircon crystals from the Graciosa A-type granites and syenites.

The Graciosa A-type granites and syenites have enriched, crust-like Hf isotopic compositions, especially the subalkaline granites. Nevertheless, the zircon $\delta^{18}O$ values, mainly between 4.7 and 6.0‰, are akin to values typically found in mantle zircon (Valley et al., 1998; Figs. 8, 12), in agreement with our above chemical evidence (Fig. 11a). Furthermore, the occurrence of coeval dioritic and gabbroic rocks in many plutons from the province (Serra da Graciosa, Corupá, Rio Negro, Palermo; Fig. 1; Vlach et al., 2011) attests for the involvement of enriched mantle-derived melts (Fig. 12), as for the contemporaneous Itu A-type Province to the north (Fig. 1; Janasi et al., 1993, 2009). Elevated $\delta^{18}O$ values like those locally found in sample MR-161 (Quiriri Pluton) and in the Serra do Paratiú/Cordeiro Pluton may arguably result from intracrustal recycling. However, the most potential contaminants should be the Archean and Paleo- to Neoproterozoic basement rocks of the Luis Alves and Curitiba microplates, and the Paranaguá Terrain, and these have similar zircon oxygen isotope compositions ($\delta^{18}O$ = 3.8–6.4‰; Valley et al., 2005). Alternatively, these elevated $\delta^{18}O$ values may be explained by low temperature interaction with meteoric water (Roberts and Spencer, 2015).

The studied rocks are also characterized by relatively high potassium contents (K_2O/Na_2O = 0.7–4.6) and their geochemical signatures are akin to the A2-type granites in the classification of Eby (1992), which have geochemical affinities similar to island arc basalts (IAB), suggesting granites related to sources previously modified by subduction-related fluids. Moreover, as many other A-type granites worldwide, some Graciosa granites are high heat-producing granites, with an average radiogenic heat production (A) of 3.0 ± 0.9 μWm^{-3}, and values as high as 7.1 μWm^{-3} (our unpublished data; Vilalva and Vlach, 2014). These values are much higher than average continental crust (A = 1.0–1.2 μWm^{-3}; Bea, 2012) and ultimately reflect the enrichment of heat-producing elements (K, Th, U) in the sources due to metasomatic reactions driven by alkali-enriched fluids, either in the lithospheric mantle or in the overlying lower continental crust (Bea, 2012; Martin, 2006; Vollmer, 1987).

Models to explain metasomatism of a sterile lithospheric mantle in a post-collisional/extensional environment involve mainly the circulation of slab-derived fluids from previous subducted materials. At the same time, the high melting temperatures necessary for the generation of A-type magmas are provided by upwelling of the asthenosphere following the lithospheric delamination after slab break-off (Davies and von Blanckenburg, 1995; Jiang et al., 2018; Li et al., 2014). Contributions from metasomatized mantle to the post-collisional magmatism in S-SE Brazil were advocated, for instance, by Janasi et al. (1993, 2009) and Vlach (1993) for the Itu A-type Province, and by Sommer et al. (2006) for the generation of shoshonitic and mildly alkaline (A-type) bimodal volcanism in post-collisional basins in Southernmost Brazil (Fig. 1). Alternatively, Martin (2006) proposed that mantle upwelling in extensional environments (mainly continental rifts) leads to mantle degassing and subsequent melt. The released alkali- and silica-bearing fluids would metasomatize the lower crust by fenitization type reactions (Vollmer, 1987; Woolley, 1987), and the resulting fertile assemblages can melt to give A-type magmas.

Although both models are plausible for the generation of the Graciosa A-type magmatism, we understand that Martin's model is more suitable for anorogenic granites associated to rifting in continental areas, as pointed out by Nardi and Bitencourt (2009). Therefore, here we explain the origin of the Graciosa granites and syenites through partial

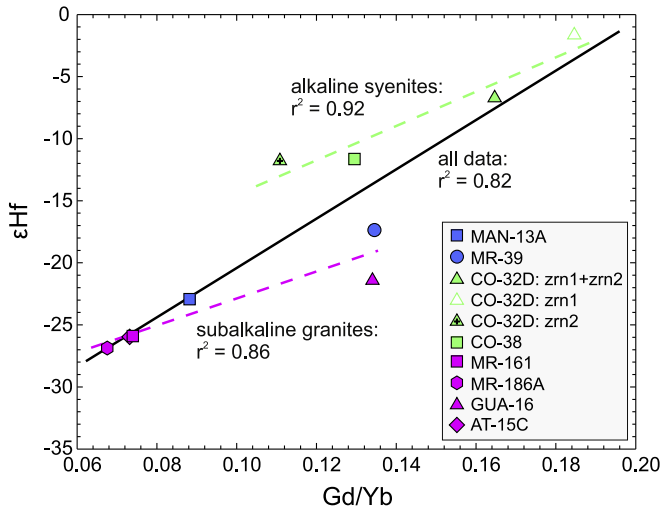

Fig. 13. Binary plot ε_{Hf} vs Gd/Yb ratio for zircon crystals from the Graciosa A-type granites and syenites.

melting of a metasomatized mantle. In this model, the lithospheric mantle becomes fertilized by the introduction of terrigenous sediments, and slab-derived fluids in previous subduction zones, as the ones represented by the Piên-Mandirituba Batholith (between the Luis Alves and Curitiba microplates), and the late-collisional suites in the Paranaguá Terrain (e.g. Basei et al., 2008, 2009; Passarelli et al., 2018). Arguably, this would impart the IAB chemical signatures recorded by the whole-rock compositions (e.g., Jiang et al., 2018), a decrease in ε_{Hf} values, and no marked effect on the $\delta^{18}O$ mantle signature (Roberts and Spencer, 2015), for the A2-type granites and syenites of the Graciosa Province.

The trace element signatures of the Graciosa zircon crystals characterized by elevated Gd/Yb ratios imply high involvement of mantle components in the melts generation. When plotted against the ε_{Hf} values, the Gd/Yb ratio in zircon correlates negatively with increasing, crust-like Hf isotopic compositions (i.e., more negative ε_{Hf} values) from the Corupá syenites to the subalkaline granites (Fig. 13). This correlation is compatible with progressively higher crustal contamination in the generation of these rocks. Nevertheless, Hf data alone cannot differentiate whether such crustal contamination occurs through mantle recycling (source contamination) or through intracrustal recycling (Roberts and Spencer, 2015). In this context, the presence of inherited Archean crystal cores in the Desemborque Pluton (sample GUA-16), as well as the local occurrence of centimetric to metric basement xenoliths in some of the subalkaline plutons (e.g., Quiriri) may argue in favor of some degree of crustal contamination during the magmatic evolution of the Graciosa magmatism.

In summary, both the trace element and isotopic signatures are compatible with generation of the A2-type Graciosa granites and syenites through partial melting of lithospheric metasomatized mantle, followed by variable degrees of crustal contamination at depth. Mantle upwelling in an extensional post-collisional tectonic regime would provide the needed heat for the melting of the above lithospheric mantle.

6.5. Geotectonic implications

Well-established tectonic models for southeastern Brazil, in the region between the states of São Paulo and Santa Catarina, assume that geological evolution for the area records the last collisional episodes of the Brasiliano (Ediacaran)/Pan-African Orogeny, and the closure of the Adamastor ocean during assembly of Western Gondwana (e.g. Basei et al., 2009; Heilbron et al., 2004; Passarelli et al., 2018). The mosaic of blocks in the region (Fig. 1) consolidated between 630 and 600 Ma, when several magmatic arcs were active; the high-K calc-alkaline Piên-Mandirituba Suite, and the late-collisional suites in the Paranaguá Terrain (Fig. 1; Basei et al., 2008, 2009). U-Pb geochronological data for these rocks (Cury, 2009; Passarelli et al., 2009 and references therein) point to an interval for emplacement and crystallization mainly between 590 and 615 Ma, suggesting a slightly younger age for the amalgamation of these blocks at ~590 Ma (Vlach et al., 2011). Alternatively, Almeida et al. (2010, 2012) proposed a model involving extensional stresses caused by mantle thermal anomalies, repeatedly interrupted by compressional events causing strike-slip deformation.

Apart from the tectonic model, the geochronological data reported here, along with previous age determinations (Fig. 9) indicate that the Graciosa magmatism was emplaced in a post-collisional extensional regime related to the geodynamic evolution of the south-southeastern part of the Gondwana supercontinent. This occurred mainly at ~580 Ma, a few million years subsequent the late-collisional magmatism.

7. Conclusions

Based on U-Pb geochronologic results, trace element abundances, and Hf and O isotopic compositions of zircon from representative samples of alkaline and subalkaline granitic and syenitic plutons from the A-type Graciosa Province (Southern Brazil), the following conclusions can be drawn in relation to the timing of their crystallization, petrogenesis and geodynamic settings within this region of Brazil:

1) The emplacement, petrogenetic evolution and crystallization of the province-forming intrusions occurred within a maximum time span of ~9 Ma; and the magmatic peak was at ~580 Ma.
2) The peralkaline Mandira Massif, cropping out at the northeastern-most area of the Graciosa Province, represents the latest magmatic episode; this may suggest a fast-magmatic focus migration within the province, from southwestern to northeastern.
3) Zircon Hf abundances may be used to distinguish between zircon from subalkaline/aluminous (Hf > 11,000 ppm) and those from alkaline granites and syenites (Hf < 11,000 ppm).
4) Zircon crystallization took place under more oxidizing conditions for the subalkaline granites compared to those for the alkaline lithotypes, at temperatures mainly between 700 and 910 °C.
5) Trace element signatures in zircon, particularly for Hf, U, Nb, and the REEs indicate contributions from both relatively enriched mantle and crustal components to the province magmatism.
6) Zircon Hf and O isotope signatures are compatible with the hypothesis that magmas were originated through partial melting of metasomatized lithospheric mantle sources, followed by variable degrees of crustal contamination at depth.

Acknowledgments

This work was financed by the São Paulo Research Foundation – FAPESP (Proc. 08/00562-0), the National Counsel of Technological and Scientific Development – CNPq (Proc. 307583/2008-2 and 142838/2007-1), and in part by the Coordenação de Aperfeiçoamento de Pessoal de Nível Superior – Brasil (CAPES) – Finance Code 001. The authors thank Dr. Xian-Hua Li for editorial handling, and Dr. Bernard Bonin and an anonymous reviewer for their useful and constructive comments that improved the manuscript. Dr. Fernando Corfu is also acknowledged for his comments and suggestions on a previous draft of the manuscript.

Appendix A. Supplementary data

Supplementary data to this article can be found online at https://doi.org/10.1016/j.lithos.2019.05.001.

References

Almeida, R.P., Janikian, L., Fragoso-César, A.R.S., Fambrini, G.L., 2010. The Ediacaran to Cambrian rift system of Southeastern South America: tectonic implications. J. Geol. 118, 145–161.

Almeida, R.P., Santos, M.G.M., Fragoso-César, A.R.S., Janikian, L., Fambrini, G.L., 2012. Recurring extensional and strike-slip tectonics after the Neoproterozoic collisional events in the Southern Mantiqueira province. An. Acad. Bras. Cienc. 84, 5–8.

Ballard, J.R., Palin, J.M., Campbell, I.H., 2002. Relative oxidation states of magmas inferred from $Ce^{(IV)}/Ce^{(III)}$ in zircon: application to porphyry copper deposits of northern Chile. Contrib. Mineral. Petrol. 144, 347–364.

Basei, M.A.S., Frimmel, H.E., Nutman, A.P., Preciozzi, F., 2008. West Gondwana amalgamation based on detrital zircon ages from Neoproterozoic Ribeira and Dom Feliciano belts of South America and comparison with coeval sequences from SW Africa. J. Geol. Soc. Lond. 294, 239–256.

Basei, M.A.S., Nutman, A.P., Siga Jr., O., Passarelli, C.R., Drukas, C.O., 2009. The evolution and tectonic setting of the Luis Alves Microplate of southeastern Brazil: an exotic terrane during the assembly of western Gondwana. Developments in Precambrian Geology 16, 273–291.

Bea, F., 2012. The sources of energy for crustal melting and the geochemistry of heat-producing elements. Lithos 153, 278–291.

Blichert-Toft, J., 2008. The Hf isotopic composition of zircon reference material 91500. Chem. Geol. 253, 252–257.

Bonin, B., 2007. A-type granites and related rocks: Evolution of a concept, problems and prospects. Lithos 97, 1–29.

Bouvier, A., Vervoort, J.D., Patchett, P.J., 2008. The Lu–Hf and Sm–Nd isotopic composition of CHUR: constraints from unequilibrated chondrites and implications for the bulk composition of terrestrial planets. Earth Planet. Sci. Lett. 273, 48–57.

Breiter, K., Lamarão, C.N., Borges, R.M.K., Dall'Agnol, R., 2014. Chemical characteristics of zircon from A-type granites and comparison to zircon of S-type granites. Lithos 192-195, 208–225.

Cavosie, A.J., Valley, J.W., Wilde, S.A., 2006. Correlated microanalysis of zircon: Trace element, $\delta^{18}O$, and U-Th-Pb isotopic constraints on the igneous origin of complex >3900 Ma detrital grains. Geochim. Cosmochim. Acta 70, 5601–5616.

Clairbone, L.L., Miller, C.F., Wooden, J.L., 2010. Trace element composition of igneous zircon: a thermal and compositional record of the accumulation and evolution of a large silicic batholith, Spirit Mountain, Nevada. Contrib. Mineral. Petrol. 160, 511–531.

Collins, W.J., Beams, S.D., White, A.J.R., Chappell, B.W., 1982. Nature and origin of A-type granites with particular reference to southeastern Australia. Contrib. Mineral. Petrol. 80, 189–200.

Corfu, F., Hanchar, J.M., Hoskin, P.W.O., Kinny, P., 2003. Atlas of zircon textures. In: Hanchar, J.M., Hoskin, P.W.O. (Eds.), Zircon. Reviews in Mineralogy and Geochemistry. vol. 53, pp. 469–500.

Cury, L.F., 2009. Geologia do Terreno Paranaguá. PhD's Thesis. Instituto de Geociências, Universidade de São Paulo, São Paulo, Brazil https://doi.org/10.11606/T.44.2009.tde-06072009-113335 (in Portuguese).

Davies, J.H., von Blanckenburg, F., 1995. Slab break-off: a model of lithospheric detachment and its test in the magmatism and delamination of collisional orogens. Earth Planet. Sci. Lett. 129, 85–102.

Eby, G.N., 1990. The A-type granitoids a review of their occurrence and chemical characteristics and speculations their petrogenesis. Lithos 26, 115–134.

Eby, G.N., 1992. Chemical subdivision of the A-type granitoids: petrogenetic and tectonic implications. Geology 20, 641–644.

Ferry, J.M., Watson, E.B., 2007. New thermodynamic models and revised calibrations for the Ti in-zircon and Zr-in-rutile thermometers. Contrib. Mineral. Petrol. 154, 429–437.

Frei, D., Gerdes, A., 2009. Precise and accurate in situ U-Pb dating of zircon with high sample throughput by automated LA-SF-ICP-MS. Chem. Geol. 261, 261–270.

Frost, C.D., Frost, B.R., 2011. On ferroan (A-type) granites: their compositional variability and modes of origin. J. Petrol. 52, 39–53.

Frost, B.R., Barnes, C.G., Collins, W.J., Arculus, R.J., Frost, C.D., 2001. A geochemical classification for granitic rocks. J. Petrol. 42, 2033–2048.

Fu, B., Mernagh, T.P., Kita, N.T., Kemp, A.I.S., Valley, J.W., 2009. Distinguishing magmatic zircon from hydrothermal zircon: a case study from the Gidginbung high-sulphidation Au–Ag–(Cu) deposit, SE Australia. Chem. Geol. 259, 131–142.

Garcia, R.P., 2015. Evolução magmática e hidrotermal de granitos de "tipo-A" reduzidos: o exemplo do Pluton Desemborque, Maciço Guaraú, SP. Master's Dissertation. Instituto de Geociências, Universidade de São Paulo, São Paulo, Brazil https://doi.org/10.11606/D.44.2015.tde-17062015-092009 (in Portuguese).

Garin, Y., Vlach, S.R.F., Tassinari, C.C.G., 2003. Sr and Nd isotope signatures of A-type alkaline syenites, granites, and associated diorites and hybrid rocks from the Corupá Massif (SC), Serra do Mar Province, S Brazil, in: 4th South American Symposium on Isotope Geology, Salvador, Brazil. CBPM/IRD. Short Papers 2, pp. 556–559. Available online at http://horizon.documentation.ird.fr/exl-doc/pleins_textes/divers17-05/010039206.pdf.

Griffin, W.L., Pearson, N.J., Belousova, E.A., Jackson, S.R., van Achterbergh, E., O'Reilly, S.Y., Shee, S.R., 2000. The Hf isotope composition of cratonic mantle: LA–ICP–MS analysis of zircon megacrysts in kimberlites. Geochim. Cosmochim. Acta 64, 133–147.

Grimes, C.B., John, B.E., Kelemen, P.B., Mazdab, F., Wooden, J.L., Cheadle, M.J., Hanghøj, K., Schwartz, J.J., 2007. The trace element chemistry of zircons from oceanic crust: a method for distinguishing detrital zircon provenance. Geology 35, 643–646.

Grimes, C.B., Wooden, J.L., Cheadle, M.J., John, B.E., 2015. "Fingerprinting" tectonomagmatic provenance using trace elements in igneous zircon. Contrib. Mineral. Petrol. 170 (46).

Gualda, G.A.R., Vlach, S.R.F., 2007a. The Serra da Graciosa A-type granites and syenites, southern Brazil. Part 1: regional setting and geological characterization. An. Acad. Bras. Cienc. 79, 405–430.

Gualda, G.A.R., Vlach, S.R.F., 2007b. The Serra da Graciosa A-type Granites and Syenites, southern Brazil. Part 2: petrographic and mineralogical evolution of the alkaline and aluminous associations. Lithos 93, 310–327.

Heilbron, M., Pedrosa-Soares, A., Campos Neto, M.C., Silva, L.C., Trouw, R.A.J., Janasi, V.A., 2004. Província Mantiqueira. In: Mantesso-Neto, V., Bartorelli, A., Carneiro, C.D.R., Brito-Neves, B.B. (Eds.), Geologia do Continente Sul-Americano: Evolução da Obra de Fernando Flávio Marques de Almeida. Beca, São Paulo, Brazil, pp. 203–234 (in Portuguese).

Hoskin, P.W.O., 2005. Trace-element composition of hydrothermal zircon and the alteration of Hadean zircon from the Jack Hills, Australia. Geochim. Cosmochim. Acta 69, 637–648.

Hoskin, P.W.O., Schaltegger, U., 2003. The composition of zircon and igneous and metamorphic petrogenesis. In: Hanchar, J.M., Hoskin, P.W.O. (Eds.), Zircon. Minerological Society of America Reviews in Mineralogy and Geochemistry. vol. 53, pp. 27–62.

Janasi, V.A., Vlach, S.R.F., Ulbrich, H.H.G.J., 1993. Enriched-mantle contributions to the Itu Granitoid Belt, Southeastern Brazil: evidence from K-rich diorites and syenites. An. Acad. Bras. Cienc. 65 (Suppl. 1), 107–118.

Janasi, V.A., Vlach, S.R.F., Campos Neto, M.C., Ulbrich, H.H.G.J., 2009. Associated A-type subalkaline and high-K calc-alkaline granites in the Itu Granite Province, SE Brazil: petrological and tectonic significance. Can. Mineral. 47, 1505–1526.

Jiang, X.Y., Ling, M.X., Wu, K., Zhang, Z.K., Sun, W.D., Sui, Q.L., Xia, X.P., 2018. Insights into the origin of coexisting A1-and A2-type granites: implications from zircon Hf-O isotopes of the Huayuangong intrusion in the lower Yangtze River Belt, eastern China. Lithos 318, 230–243.

Jourdan, A.-L., Vennemann, T.W., Mullis, J., Ramseyer, K., 2009. Oxygen isotope sector zoning in natural hydrothermal quartz. Mineral. Mag. 73, 615–632.

Kaul, P.F.T., Cordani, U.G., 2000. Geochemistry of the Serra do Mar granitoid magmatism and tectonic implications, southern Brazil. Revista Brasileira de Geociências 30, 115–119.

Li, H., Ling, M.X., Ding, X., Zhang, H., Li, C.Y., Liu, D.Y., Sun, W.D., 2014. The geochemical characteristics of Haiyang A-type granite complex in Shandong, eastern China. Lithos 200, 142–156.

Liégeois, J.P., 1998. Preface – some words on the postcollisional magmatism. Lithos 45, xv–xvii.

Ludwig, K.R., 2012. User's Manual for Isoplot 3.75, A Geochronlogical Toolkit for Microsoft Excel. vol. 5. Berkeley Geochronology Center Special Publication.

Martin, R.F., 2006. A-type granites of crustal origin ultimately result from open-system fenitization-type reactions in an extensional environment. Lithos 91, 125–136.

Miller, J.S., Matzel, J.E.P., Millwer, C.F., Burgess, S.D., Miller, R.B., 2007. Zircon growth and recycling during the assembly of large, composite, arc plutons. J. Volcanol. Geotherm. Res. 167, 282–299.

Nardi, L.V.S., Bitencourt, M.F., 2009. A-type granitic rocks in post-collisional settings in southernmost Brazil: their classification and relationship with tectonics and magmatic series. Can. Mineral. 47, 1493–1503.

Passarelli, C.R., Basei, M.A.S., Siga Jr., O., Sato, K., Sproesser, W.M., Loios, V.A., 2009. Dating minerals by ID-TIMS geochronology at times of in situ analysis: selected case studies from the CPGeo-IGc-USP laboratory. An. Acad. Bras. Cienc. 81, 73–97.

Passarelli, C.R., Basei, M.A.S., Siga Jr., O., Harara, O.M.M., 2018. The Luis Alves and Curitiba Terranes: continental fragments in the Adamastor Ocean. Geology of Southwest Gondwana. Springer, Cham, pp. 189–215.

Patiño-Douce, A.E., 1997. Generation of metaluminous A-type granites by low-pressure melting of calc-alkaline granitoids. Geology 25, 743–746.

Pearson, N.J., Griffin, W.L., O'Reilly, S.Y., 2008. Mass fractionation correction in laser ablation multiple-collector ICP-MS: implications for overlap corrections and precise and accurate in-situ isotope ratio measurement. Laser Ablation-ICP-MS in the Earth Sciences: current practices and outstanding issues, Edited by Paul Sylvester. vol. 40. Mineralogical Association of Canada Short Course Series, pp. 93–1156.

Pupin, J.P., 1980. Zircon and granite petrology. Contrib. Mineral. Petrol. 73, 207–220.

Roberts, N.M., Spencer, C.J., 2015. The zircon archive of continent formation through time. Geol. Soc. Lond. Spec. Publ. 389 (1), 197–225.

Sambridge, M.S., Compston, W., 1994. Mixture modeling of multi-component data sets with application to ion-probe zircon ages. Earth Planet. Sci. Lett. 128, 373–390.

Scaillet, B., Holtz, F., Pichavant, M., 2016. Experimental constraints on the formation of silicic magmas. Elements 12 (2), 109–114.

Sharp, Z.D., 1990. A laser-based microanalytical method for the in situ determination of oxygen isotope ratios of silicates and oxides. Geochim. Cosmochim. Acta 54, 1353–1357.

Siégel, C., Bryan, S.E., Allen, C.M., Gust, D.A., 2018. Use and abuse of zircon-based thermometers: a critical review and a recommended approach to identifiy antecrystic zircons. Earth Sci. Rev. 176, 87–116.

Siga Jr., O., Basei, M.A.S., Machiavelli, A., 1993. Evolução geotectônica da porção NE de Santa Catarina e SE do Paraná, com base em interpretações geocronológicas. Revista Brasileira de Geociências 23, 215–223 (in Portuguese).

Simonetti, A., Neal, C.R., 2010. In-situ chemical, U-Pb dating, and Hf isotope investigation of megacrystic zircons, Malaita (Solomon Islands): evidence for multi-stage alkaline magmatic activity beneath the Ontong Java Plateau. Earth Planet. Sci. Lett. 295, 251–261.

Simonetti, A., Heaman, L.M., Hartlaub, R.P., Creaser, R.A., McHattie, T.G., Böhm, C., 2005. U-Pb dating of zircon by laser ablation-MC-ICP-MS using a new multiple ion counting-faraday collectory array. Journal of Analytical Atomic Spectroscopy 20, 677–686.

Söderlund, U., Patchett, P.J., Vervoort, J.D., Isachsen, C.E., 2004. The ^{176}Lu decay constant determined by Lu–Hf and U–Pb isotope systematic of Precambrian mafic intrusions. Earth Planet. Sci. Lett. 219, 311–324.

Sommer, C.A., Lima, E.F., Nardi, L.V.S., Liz, J.D., Waichel, B.L., 2006. The evolution of Neoproterozoic magmatism in Southernmost Brazil: shoshonitic, high-K tholeiitic

and silica-saturated, sodic alkaline volcanism in post-collisional basins. An. Acad. Bras. Cienc. 78, 573–589.
Stern, R.A., Amelin, Y., 2003. Assessment of errors in SIMS zircon U–Pb geochronology using a natural zircon standard and NIST SRM 610 glass. Chem. Geol. 197, 111–142.
Trail, D., Watson, E.B., Tailby, N.D., 2012. Ce and Eu anomalies in zircon as proxies for the oxidation state of magmas. Geochim. Cosmochim. Acta 97, 70–87.
Turner, S.P., Foden, J.D., Morrison, R.S., 1992. Derivation of some A-type magmas by fractionation of basaltic magma: an example from the Padthaway Ridge, South Australia. Lithos 28, 151–179.
Valley, J.W., Kinny, P.D., Schulze, D.J., Spicuzza, M.J., 1998. Zircon megacrysts from kimberlite: oxygen isotope variability among mantle melts. Contrib. Mineral. Petrol. 133, 1–11.
Valley, J.W., Lackey, J.S., Cavosie, A.J., Clechenko, C.C., Spicuzza, M.J., Basei, M.A.S., Bindeman, I.N., Ferreira, V.P., Sial, A.N., King, E.M., Peck, W.H., Sinha, A.K., Wei, C.S., 2005. 4.4 billion years of crustal maturation: oxygen isotope ratios of magmatic zircon. Contrib. Mineral. Petrol. 150, 561–580.
van Achterbergh, E., Ryan, C., Jackson, S., Griffin, W., 2001. Appendix 3: Data reduction software for LA-ICP-MS. In: Sylvester, P. (Ed.), Laser-Ablation-ICPMS in the Earth Sciences. vol. 29. Mineralogical Association of Canada Short Course, pp. 239–243.
Vilalva, F.C.J., Vlach, S.R.F., 2014. Geology, petrography and geochemistry of the A-type granites from the Morro Redondo Complex (PR-SC), South Brazil, Graciosa Province. An. Acad. Bras. Cienc. 86, 85–116.
Vlach, S.R.F., 1993. Geologia e petrologia dos granitóides de Morungaba/SP. PhD Thesis. Instituto de Geociências, Universidade de São Paulo, São Paulo, Brazil https://doi.org/10.11606/T.44.1993.tde-15042013-112501 (in Portuguese).
Vlach, S.R.F., 2012. Micro-structural and compositional variations of hydrothermal epidote-group minerals from a peralkaline granite, Corupá Pluton, Graciosa Province, South Brazil, and their petrological implications. An. Acad. Bras. Cienc. 84, 407–426.
Vlach, S.R.F., Gualda, G.A.R., 2007. Allanite and chevkinite in A-type granites and syenites of the Graciosa Province, southern Brazil. Lithos 97, 98–121.
Vlach, S.R.F., Siga Jr., O., Harara, O.M.M., Gualda, G.A.R., Basei, M.A.S., Vilalva, F.C.J., 2011. Crystallization ages of the A-type magmatism of the Graciosa Province (Southern Brazil): constraints from the zircon U-Pb (ID-TIMS) dating of coeval K-rich gabbro-dioritic rocks. J. S. Am. Earth Sci. 32, 407–415.
Vogado, F.P., Ferreira, F.J.P.F., Vlach, S.R.F., Negri, F.A., 2011. O Maciço Granítico Alto-Turvo (SP/PR), Província Graciosa: Análise de padrões aero-gamaespectrométricos. 12th Simpósio de Geologia do Sudeste, Nova Friburgo, Brazil. SBG. Anais. 57 (in Portuguese; available online at http://sbg-mg.org.br/novosite/wp-content/uploads/2017/11/XII-SGS.pdf).
Vollmer, R., 1987. Metasomatism of the continental lithosphere: simulation of isotope and element abundance behaviour and case studies. In: Helgeson, H.C. (Ed.), Chemical Transport in Metasomatic Processes. Springer, Dordrecht, pp. 53–90.
Watson, E.B., Harrison, T.M., 2005. Zircon thermometer reveals minimum melting conditions on earliest. Earth Sci. 308, 841–844.
Whalen, J.B., Currie, K.L., Chappell, B.W., 1987. A-type granites: geochemical characteristics, discrimination and petrogenesis. Contrib. Mineral. Petrol. 95, 407–419.
Woodhead, J.D., Hergt, J.M., 2005. A preliminary appraisal of seven natural zircon reference materials for in situ Hf isotope determination. Geostand. Geoanal. Res. 29, 183–195.
Woolley, A.R., 1987. Lithosphere metasomatism and the petrogenesis of the Chilwa Province of alkaline igneous rocks and carbonatites, Malawi. J. Afr. Earth Sci. 6, 891–898.
Yang, J.H., Wu, F.Y., Chung, S.L., Wilde, S.A., Chu, M.F., 2006. A hybrid origin for the Qianshan A-type granite, Northeast China: geochemical and Sr–Nd–Hf isotopic evidence. Lithos 89, 89–106.